Technical Report 469

Automatic Orbit Control of the Lincoln Experimental Satellite LES-6

A. A. Braga-Illa

10 July 1969

Prepared under Electronic Systems Division Contract AF 19(628)-5167 by

Lincoln Laboratory
MASSACHUSETTS INSTITUTE OF TECHNOLOGY
Lexington, Massachusetts

MASSACHUSETTS INSTITUTE OF TECHNOLOGY
LINCOLN LABORATORY

AUTOMATIC ORBIT CONTROL OF THE LINCOLN EXPERIMENTAL SATELLITE LES-6

A. A. BRAGA-ILLA

Group 63

TECHNICAL REPORT 469

10 JULY 1969

LEXINGTON MASSACHUSETTS

The work reported in this document was performed at Lincoln Laboratory, a center for research operated by Massachusetts Institute of Technology, with the support of the Department of the Air Force under Contract AF 19(628)-5167.

ABSTRACT

This report discusses the autonomous orbit control system launched aboard the synchronous communications satellite LES-6 in late 1968. The topics presented include the motivation for automatic orbit control, the measurement techniques, observability and controllability, the design of a variable limit-cycle system, automatic station acquisition, simulation, and testing. The history of the development of this control system is emphasized, and the early flight results are discussed.

Accepted for the Air Force
Franklin C. Hudson
Chief, Lincoln Laboratory Office

CONTENTS

AUTOMATIC ORBIT CONTROL OF THE LINCOLN EXPERIMENTAL SATELLITE LES-6

I. INTRODUCTION

For several years, satellites have been used to establish radio communication links between stations located on the surface of the earth. Radio signals transmitted by one station are received by the satellite, amplified, and retransmitted to one or more terminal points on the ground. Normally, line-of-sight transmission is required, so that only those stations which would be visible to a hypothetical observer on the satellite can be connected by this type of radio link.

A major requirement for any communications system is that the link between stations be uninterrupted, so that transmission of information between the terminals is possible at all times. This need has led to the introduction of "synchronous" satellites which revolve around the earth at an average angular rate equal to that at which the earth spins around its polar axis. As is well known, the orbital period of a satellite is related to its total energy, which in turn is a function of the orbital major axis. By appropriately choosing the latter, the satellite period can be made equal to one sidereal day. Furthermore, if the orbit is equatorial and circular, the satellite is geostationary, or motionless, relative to an observer on the earth. It follows that one way of avoiding interruption of transmission due to the motion of the satellite with respect to the ground terminals is to place the spacecraft in a circular, equatorial, synchronous orbit.

Unfortunately, this ideal situation cannot be achieved permanently. A synchronous satellite is subject to forces which tend to displace it from the geostationary position:[1-5] a stable synchronous orbit exists at only two earth longitudes, about 107° West (over the Pacific Ocean) and 73° East (over the Indian Ocean). In general, the satellite has a long-term pendular motion about the initial synchronous position, which must be opposed by a thruster on the satellite. On the first synchronous satellites, the thruster was commanded by a signal from the ground, after a difference between the actual and the desired satellite positions had been detected by tracking, until the desired drift velocity and position were obtained.

A completely automatic and self-contained technique has been realized for the first time on the Lincoln Experimental Satellite LES-6, a communications satellite that was launched successfully on 26 September 1968. In this system, the angular position error is measured on the satellite itself and thrusters are fired according to a correction sequence determined by a digital controller on board. This approach (a) eliminates tracking and commanding, and (b) is potentially more accurate than the ground-command method. The satellite can also be made to acquire new longitudinal positions by changing an internal reference, so that it can follow new stations in a preprogrammed sequence or upon receipt of simple instructions from the ground.

The use of an Automatic Orbit Control system significantly reduces the need for ground tracking. We believe that this is a primary economic incentive to the use of these techniques in the future. To appreciate the fact, it is instructive to consider our own experience in determining the orbit of LES-6, using a 30-foot UHF antenna in Lexington, Massachusetts. The data recorded by the ground station are satellite range, obtained from the round-trip time of a signal sent through the satellite repeater, and elevation and azimuth angles, derived directly (and rather inaccurately) by pointing the antenna for maximum received signal. These measurements, which last several minutes, are repeated hourly for 30 consecutive hours and are then processed

by an Orbit Determination Program, which performs a least-square fit on the data to yield one value of satellite position and drift. This orbit determination is thus a non-trivial burden, which of course becomes more significant as the number of satellites to be tracked increases, or when the ground station must be used for purposes other than satellite tracking. Ground station saturation is, therefore, one of the problems that Automatic Orbit Control, done directly from the satellite, will alleviate.

The second advantage of an Automatic Orbit Control system, i.e., that of accuracy, is still to be proven. In fact, one major aim in launching the LES-6 system has been to collect information that will enable us to design high-accuracy second generation systems. Our goal on LES-6 was a rather modest ±2 degrees in steady-state longitude accuracy: this is amply sufficient for earth-coverage microwave systems, and is indeed very satisfactory, as is known to those who have experience in synchronous satellite orbit control. The longitudinal accuracy which can be achieved with ground tracking techniques depends on (a) the orbit determination accuracy, and (b) the time interval between corrections. The Syncom satellites, for example, have achieved accuracies of 2 degrees, with corrections about every 30 days. If the orbit is measured and controlled directly from the satellite, the constraints imposed on the correction interval by ground station limitations are removed. Greater orbit control accuracy is important for satellites using narrow-beam, i.e., high-gain, antennas. A second incentive for accurate longitude control is connected to the use of many synchronous satellites closely spaced in longitude: in the future there will be a problem of allocation of "synchronous orbit space," especially in the neighborhood of some preferred longitudes. In this report we discuss some preliminary statistical results obtained from sun and earth sensors.

The work that is presented here refers to near-circular orbits, and the flight data were collected from the synchronous equatorial satellite LES-6. However, these ideas, and those which will develop from our own and others' experience, will probably be applied to other types of orbits. Earth-resources satellites and large unmanned orbital platforms may become a reality. As the number of active satellites increases and improvements in solar power systems lengthen their useful lives, on-board control of the orbit parameters will become increasingly important. The acceptance of automatic techniques depends, of course, on their reliability. At the time of this writing, the Automatic Orbit Control system of LES-6 had operated properly for eleven months. During this time, the Pulsed Plasma Thrusters operated for about 3,500 hours. We hope to be able to demonstrate that the system can control the orbit automatically for several years.

Automatic orbit control has not been attempted until now, although self-contained methods have been proposed in the literature by several authors. Some of these studies include applications of filtering theory, especially Kalman's, to this problem. The explanation of the delay in realization lies, at least in part, in the complexity of the orbit determination techniques which had been proposed until recently. Reliability, weight, and power limitations have made all the systems proposed impractical for today's communications satellites.

It is interesting to review briefly the development of self-contained navigation ideas, which naturally center around the problem of determining the orbit from autonomous data. A good general survey up to 1965 is made by Gansler,[6,7] who considers the classic distinction between preliminary determination and updating of the orbit.† The existing literature on the subject of

† Gansler's evoluation of the characteristics of o "typicol" self-cantained navigotian system, excluding the propulsion equipment, is that it will weigh 87 pounds and require 218 watts. The LES-6 system weighs 4 pounds and uses 120 milliwatts.

on-board orbit determination falls in three categories: (a) discussions of instruments with which to observe satellite position and dynamic coordinates, (b) elaborations of the orbit equations, (c) applications of filtering theory, especially Kalman's. The first group includes the many types of sensors, star trackers, inertial platforms, and dynamometers which have been proposed but will not be discussed here. The best paper in the second group is by Gersten and Schwarzbein,[8] who give formulas for the orbital elements as a function of various combinations of measurements of satellite altitude, anomaly, and velocity components. The difficulty is that the relationships are transcendental equations which, even if expressed in closed form, require relatively sophisticated computation systems to obtain reasonable accuracy. The same authors examined some additional cases[9] in which intervals of time as well as dynamic coordinates are measured; they suggest that the equation of motion be solved repeatedly for different values of orbital major axis until the time measurements agree with the computed results. McAllister and Wagner[10] give the equations of motion for impulsive perturbations of the dynamic coordinates of a satellite in a circular orbit as a state transition matrix. Several authors apply Kalman's statistical filtering theory[11-20] to the determination of orbits. Battin[13] also solved the problem of selecting the best star to use as a reference in making angular measurements. Frazier, et al.,[14] examined the possibility of approximating the values of satellite anomaly and the subtense of the principal body with polynomials in time and found that, in general, it is preferable to use the linearized form of the known dynamic equations to smooth the data, leading to more complex data processing requirements.

In 1965, W. E. Morrow of Lincoln Laboratory proposed that a simple combination of sun and earth sensors could be used to determine the satellite "high-noon" position in orbit; a stable oscillator could furnish an appropriate reference for the motion in sidereal space of any earth meridian, and the correction for sun transit time effects could be performed digitally on board. Shortly thereafter, the author, while studying the problem of the automatic pointing of a communication antenna from a near-circular orbit to earth, proposed simple methods of orbit determination and reconstruction[21] which were particularly suited for implementation on a satellite. The present LES-6 Automatic Orbit Control system has evolved from these ideas.

Section II of this report discusses the longitudinal perturbations of synchronous satellite orbits. Section III deals with the orbit determination problem, for small eccentricity orbits; solutions requiring linear combinations of times of flight are discussed. Section IV examines the observability and controllability issues from the point of view of modern control theory. Section V describes the finite-state controller which was actually flown on LES-6 and discusses the automatic station-acquisition maneuver. Section VI deals briefly with the hardware implementation, the simulation studies, the choice of the integration routines and step size, the random and deterministic error simulation, and the testing of the flight system. Section VII discusses the dynamic behavior in orbit and several statistical hypotheses on sensor errors.

II. EFFECTS OF EQUATORIAL ELLIPTICITY ON SYNCHRONOUS ORBITS

The influence of the asymmetries of the earth's gravitational potential on the motion of satellites has been studied by several authors. For equatorial synchronous satellites, the most important effect is that due to the "equatorial eccentricity"† which is of the order of 10^{-5}. We

† One should consider that this is simply a convenient way of interpreting the measured gravitational potential in the equatorial plane. In fact, for an eccentricity of 10^{-5}, the difference between major and minor semiaxes is only about 380 feet.

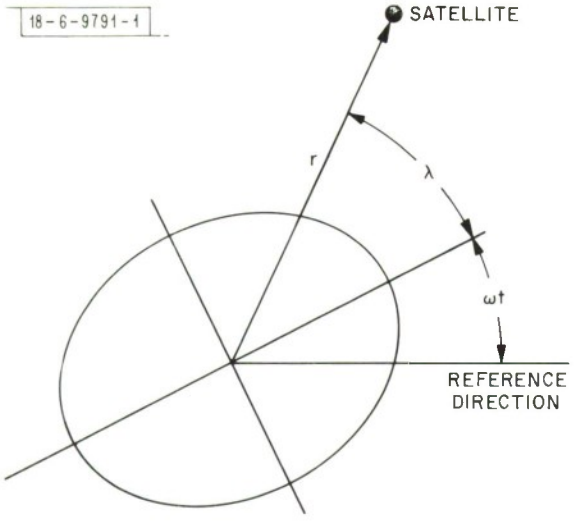

Fig. 1. Reference system for elliptic earth.

collect here some of the important results, following mainly Ref. 1. We further develop the "weak coupling" approximation and show it to be valid for the satellite motion sampled once per day.

Stable synchronous orbits exist only at the two longitudes which correspond to the minor axis of the equatorial ellipse. The longitudes along the major axis are unstable equilibrium points. At all other longitudes, the satellite is subject to a drift acceleration and its motion exhibits a long-term pendular motion, dependent on the initial conditions, about a stable point. According to recent determinations, the minor axis is located at about 73° East. Let r, λ be defined as in Fig. 1, and let Θ be the satellite colatitude. Further, R = mean equatorial radius of the earth, J_2 = coefficient of the second zonal harmonic of the earth (which is related to the polar oblateness), and γ = ellipticity of the equator.

The kinetic energy in a coordinate frame which rotates rigidly with the earth at angular speed ω is

$$T = \frac{1}{2}\dot{r}^2 + \frac{1}{2}r^2\dot{\Theta}^2 + \frac{1}{2}r^2\sin^2\Theta\,(\dot{\lambda}+\omega)^2 \quad , \tag{II-1}$$

and the potential energy can be written[22]

$$V = -\frac{\mu}{r}\left[1 - \frac{J_2R^2}{2r^2}(3\cos^2\Theta - 1) + \frac{\gamma R^2}{2r^2}\sin^2\Theta\cos 2\lambda\right] \quad . \tag{II-2}$$

We wish to find stationary solutions $r = r_o$, $\lambda = \lambda_o$, $\Theta = \Theta_o$. From Lagrange's equations,

$$\frac{d}{dt}\frac{\partial}{\partial q_k}(T - V) = \frac{\partial}{\partial q_k}(T - V) \tag{II-3}$$

(where q_k is any of the dynamic coordinates r, λ, Θ) follows, for the stationary case,

$$\frac{\partial}{\partial q_k}(T - V) = 0 \quad ,$$

and hence the equations

$$\begin{cases} r_o\omega^2\sin^2\Theta_o - \dfrac{\mu}{r_o^2} + \dfrac{3\mu J_2R^2}{2r_o^4}(3\cos\Theta_o - 1) - \dfrac{3\mu\gamma R^2}{2r_o^4}\sin^2\Theta_o\cos 2\lambda_o = 0 \quad , & \text{(II-4)} \\ \gamma\dfrac{\mu R^2}{r_o^3}\sin^2\Theta_o\sin 2\lambda_o = 0 \quad , & \text{(II-5)} \\ \left(\dfrac{1}{2}\omega^2r_o^2 - \dfrac{3\mu J_2R^2}{2r_o^3} - \dfrac{\mu\gamma R^2}{2r_o^3}\cos 2\lambda_o\right)\sin 2\Theta_o = 0 \quad . & \text{(II-6)} \end{cases}$$

The last equation has the solutions $\Theta_o = 0$ and $\pi/2$, of which the last, corresponding to equatorial orbits, is acceptable. (This can be seen on physical grounds, or by introducing the solution $\Theta_o = 0$ in the previous equations and checking that no solution exists for r_o.) Then, from (II-5), stationary points are found to exist at longitudes 0, $\pi/2$, π, $(3/2)\,\pi$ (measured from the major axis of the equatorial ellipse). The values of r_o which correspond to these solutions are found from

$$r_o\omega^2 = \frac{\mu}{r_o^2} + \frac{3\mu J_2 R^2}{2r_o^4} \pm \frac{3\gamma\mu R^2}{2r_o^4} \qquad \text{(II-7)}$$

(the positive sign corresponds to the points on the ellipse major axis). To discuss the stability of these solutions, we write Lagrange's equations and linearize about the stationary points.

The following three equations result easily:

$$\ddot{r}_\delta - \left(1 + \frac{2\mu}{\omega^2 r_o^3} + \frac{6\mu J_2 R^2}{\omega^2 r_o^5} \pm \frac{6\mu\gamma R^2}{\omega^2 r_o^5}\right)\omega^2 r_\delta - 2r_o\omega\dot{\lambda}_\delta = 0 \quad , \qquad \text{(II-8)}$$

$$\ddot{\lambda}_\delta \pm \frac{2\gamma\mu R^2}{r_o^5}\,\lambda_\delta + 2\,\frac{\omega}{r_o}\,\dot{r}_\delta = 0 \quad , \qquad \text{(II-9)}$$

$$\ddot{\Theta}_\delta + \left(1 + \frac{3\mu J_2 R^2}{\omega^2 r_o^5} \pm \frac{\gamma\mu R^2}{\omega^2 r_o^5}\right)\omega^2\Theta_\delta = 0 \quad , \qquad \text{(II-10)}$$

in which the subscript δ indicates that the variables are variations around the stationary values.

The third equation is decoupled from the first two. The motion in Θ is harmonic with frequency $\omega/2\pi$, i.e., with daily period, given the orders of magnitude of the quantities involved.

To discuss the stability of the other two coupled equations, we find the eigenvalues of the system, in which we can make approximations remembering that $\mu/\omega^2 \simeq r_o^3$ (this can be obtained by equating the centrifugal and gravitational accelerations in synchronous orbit) and that J_2 and $\gamma \ll 1$. Then the system reduces to

$$\ddot{r}_\delta - 3\omega^2 r_\delta - 2r_o\omega\dot{\lambda}_\delta = 0 \quad , \qquad \text{(II-11)}$$

$$\frac{2\omega}{r_o}\,\dot{r}_\delta + \ddot{\lambda}_\delta \pm 2\gamma\left(\frac{R}{r_o}\right)^2\omega^2\lambda_\delta = 0 \quad . \qquad \text{(II-12)}$$

Using operator notation, the equations for the system are

$$(p^2 - 3\omega^2)\,z_1 - 2r_o\omega p z_2 = 0 \quad , \qquad \text{(II-13)}$$

$$\frac{2\omega}{r_o}\,p z_1 + (p^2 \pm c\omega^2)\,z_2 = 0 \quad , \qquad \text{(II-14)}$$

where $c = 2\gamma\,(R/r_o)^2$, from which the eigenvalues are the solutions of the characteristic equation

$$p^4 + \omega^2 p^2 \mp 3c\omega^4 = 0 \qquad \text{(II-15)}$$

or

$$p^2 = \frac{-\omega^2 \pm \omega^2 \sqrt{1 \pm 12c}}{2} \simeq \begin{cases} -\omega^2 \\ \pm 3c\omega^2 = \pm 6\gamma \left(\frac{R}{r_o}\right)^2 \omega^2 \end{cases} . \qquad \text{(II-16)}$$

The first solutions ($\pm j\omega$) are oscillatory. The second set implies instability when positive sign applies (major axis) and stability in the other case (minor axis). The solutions then include a daily component (at frequency ω) and a slow oscillation with period

$$T = \frac{r_o}{R} \frac{1}{\sqrt{6\gamma}} \simeq \frac{6.63}{\sqrt{6 \times 10^{-5}}} \simeq 850 \text{ days} .$$

By solving the system with appropriate initial conditions, Blitzer, et al., find that the trajectory in the rotating coordinate frame is a very elongated ellipse about the stable longitude. The samc study shows computer results for the complete (nonlinear) equations of motion. Since that analysis was made, the observations of synchronous satellites have confirmed its validity.†

It is interesting to discuss a further approximation to the system [(II-8), (II-9), (II-10)], which we shall call "weak coupling" and which is very important for the applications. If we assume $\ddot{r}_\delta$ small, we can write

$$\begin{cases} 3\omega r_\delta^* + 2r_o \dot{\lambda}_\delta^* = 0 , & \text{(II-17)} \\ \frac{2\omega}{r_o} \dot{r}_\delta^* + \ddot{\lambda}_\delta^* \pm 2\gamma \left(\frac{R}{r_o}\right)^2 \omega^2 \lambda_\delta^* = 0 . & \text{(II-18)} \end{cases}$$

From the first equation it is

$$\frac{r_\delta^*}{r_o} = -\frac{2}{3} \frac{\dot{\lambda}_\delta^*}{\omega} . \qquad \text{(II-19)}$$

This equation can be obtained from first principles, namely, from Kepler's third law. It relates small changes in period to small changes in semimajor axis. Taking the time derivative of (II-17) and substituting in (II-18),

$$\ddot{\lambda}_\delta^* \mp 6\gamma \left(\frac{R}{r_o}\right)^2 \omega^2 \lambda_\delta^* = 0 . \qquad \text{(II-20)}$$

Thus, we have obtained a second-order equation in the variable λ_δ^* which is decoupled from the equation in r_δ^* and which has the correct long-term motion with frequencies $\pm \sqrt{6\gamma}\,(R/r_o)\,\omega$ in the stable case.

One is then led to consider what happens if λ_δ is sampled once a day, i.e., if the daily component in the solutions is desregarded. In order to check that indeed the variables λ_δ^*, r_δ^* of the weak-coupling approximation are the values of λ_δ, r_δ sampled once per day, we can proceed as follows.

The general solution for the linearized system [Eqs. (II-11) and (II-12)] in the stable case is obtained easily

† It must be noted that luni-solar perturbations alter this picture by effectively changing the synchronous semimajor axis. Closed orbits no longer exist even at the "stable" points.

$$\lambda_\delta = A_1 e^{j\omega t} + A_2 e^{-j\omega t} + B_1 e^{+j\alpha\omega t} + B_2 e^{-j\alpha\omega t} \quad , \tag{II-21}$$

$$r_\delta = -j \frac{r_o}{2} [A_1 e^{j\omega t} - A_2 e^{-j\omega t}] - j \frac{4}{\sqrt{6}} \sqrt{\gamma}\, R [B_1 e^{j\alpha\omega t} - B_2 e^{-j\alpha\omega t}] \quad , \tag{II-22}$$

where

$$\alpha \simeq \sqrt{6\gamma}\, \frac{R}{r_o} << 1 \quad .$$

Let us consider only the values at times $t = nT_s$, where $T_s = 2\pi/\omega$, $n = 0, 1, 2, \ldots$. In particular, we can select the initial value (that is to say, the phase of the sampling) so that

$$A_1 - A_2 = 0 \quad . \tag{II-23}$$

Consider then the values of r_δ, $\ddot{r}_\delta$, and $\dot{\lambda}_\delta$ at the sampling times, which we indicate with a star:

$$r_\delta^* = -j \frac{4}{\sqrt{6}} \sqrt{\gamma}\, R [B_1 e^{j\alpha 2\pi n} - B_2 e^{-j\alpha 2\pi n}] \quad , \tag{II-24}$$

$$\ddot{r}_\delta^* = +j \frac{4}{\sqrt{6}} \sqrt{\gamma}\, R(\alpha\omega)^2 [B_1 e^{j\alpha 2\pi n} - B_2 e^{-j\alpha 2\pi n}] \quad , \tag{II-25}$$

$$\dot{\lambda}_\delta^* = j\alpha\omega [B_1 e^{j\alpha 2\pi n} - B_2 e^{-j\alpha 2\pi n}] \quad . \tag{II-26}$$

Remembering the definition of α, we obtain that $\omega^2 r_\delta^*$ and $\omega\dot{\lambda}_\delta^*$ are of order $\sqrt{\gamma}$, while $\ddot{r}_\delta^*$ is of order $(\sqrt{\gamma})^3$ and therefore negligible in (II-8). Thus, we can conclude that if one uses as variables the radius and the geocentric longitude observed once per day, one can study the satellite drift in a neighborhood of the minor axis from the simple decoupled Eqs. (II-19) and (II-20).

The previous equations and conclusions apply to motion in a neighborhood of the stationary points. It is important to establish the weak-coupling approximation for all values of longitude λ. Let us linearize about the values r_o and all derivatives equal zero, treating λ as a finite quantity. Then Eq. (II-8) remains unchanged, while (II-9) becomes

$$\frac{2\omega}{r_o} \dot{r}_\delta + \ddot{\lambda} + \frac{\gamma\mu R^2}{r_o^5} \sin 2\lambda = 0 \quad , \tag{II-27}$$

an equation which is nonlinear in λ. Let us consider linearized solutions to the previous equation. For $\lambda \simeq \lambda_o$ we can write

$$\begin{cases} \ddot{r}_\delta - 3\omega^2 r_\delta - 2r_o\omega\dot{\lambda}_\delta = 0 \quad , & \text{(II-28)} \\ \dfrac{2\omega}{r_o} \dot{r}_\delta + \ddot{\lambda}_\delta = -\dfrac{\gamma\mu R^2}{r_o^5} \sin 2\lambda_o \quad . & \text{(II-29)} \end{cases}$$

The characteristic equation is found easily,

$$p^4 + \omega^2 p^2 = 0 \quad , \tag{II-30}$$

and the general solution is

$$\begin{cases} \lambda_\delta(t) = A_1 e^{j\omega t} + A_2 e^{-j\omega t} + B_1 + B_2 t + \frac{3}{2}\frac{\gamma\mu R^2}{r_o^5}\sin 2\lambda_o \cdot t^2 \quad , & \text{(II-31)} \\ r_\delta(t) = -A_1 \frac{r_o}{2} j e^{j\omega t} + A_2 \frac{r_o}{2} j e^{-j\omega t} - 2\frac{r_o}{\omega}\frac{\gamma\mu R^2}{r_o^5}\sin 2\lambda_o \cdot t - \frac{2}{3}\frac{r_o}{\omega} B_2 \quad . & \text{(II-32)} \end{cases}$$

Sampling at $t = nT_s = (2\pi/\omega)\, n$,

$$\lambda^*_\delta(nT) = (A_1 + A_2 + B_1) + B_2 nT + \frac{3}{2}\frac{\gamma\mu R^2}{r_o^5}\sin 2\lambda_o \cdot (nT)^2 \quad . \qquad \text{(II-33)}$$

Thus the longitude sampled once per day satisfies the differential equation

$$\ddot{\lambda}^*_\delta - \frac{3\gamma\mu R^2}{r_o^5}\sin 2\lambda_o = 0 \quad . \qquad \text{(II-34)}$$

We can write the general solution to (II-27) by letting the coefficients of the linearized solution, Eq. (II-31), be functions of time:

$$\lambda^*(t) = D_0 + D_1(t) \cdot t + D_2(t) \cdot t^2 \quad , \qquad \text{(II-35)}$$

where the coefficients $D_1(t)$, $D_2(t)$ are determined by choosing different values for λ_o. Then we can conclude that the weak-coupling approximation is valid for the nonlinear equation

$$\ddot{\lambda}^*(t) - \frac{3\gamma\mu R^2}{r_o^5}\sin 2\lambda^* = 0 \quad . \qquad \text{(II-36)}$$

This is the well-known "pendulum equation" of elementary dynamics. For small excursions of λ^*, the linearized approximation, leading to parabolic motion, Eq. (II-33), can be used. As we shall see, the pendulum equation is very useful in practice, since the motion of the satellite is thus reduced to a one-dimensional problem. The radius vector is still given by (II-19). It can further be shown[3] that considering the higher-order tesseral harmonics does not essentially modify these conclusions.

III. SIMPLE METHODS TO DETERMINE NEAR-CIRCULAR ORBITS

A. General Principles

Since elliptic orbits can be described by any set of sufficient parameters, we wish to use parameters which are most easily measured with on-board instrumentation. The orbit can then be controlled by maintaining these parameters at a reference value: the computation problem, and the measurement and control problems are treated as a whole. The desired control accuracy determines the precision necessary in the measurement and in the computations, and this in turn affects the choice of the technique of orbit determination. The methods summarized here only require linear combinations of measured times of flight. The results are obtained from well-known expansions of the law of motion in terms of the orbital eccentricity ϵ to terms of the third order. Several properties of the second-order solution, which are of great practical interest, are discussed. These techniques can also be applied to the determination of the center of the earth from the satellite[21] and to circularize an orbit automatically, as seen in the following.

Sinee, as we have seen, the out-of-plane perturbations of the motion of the satellite† are deeoupled from the motion in the orbit plane, we study plane motion only.

The instrumentation needed for the measurements eonsists of an earth sensor, a sun or star sensor, and a clock. The earth sensor must determine the direction of the center of the earth, or loeal vertieal, and ean be an infrared or optieal sensor.[23-25] If an optieal sensor is used, eleetronic proeessing of its output is necessary to correct for the variation of apparent width of the earth as the earth-satellite-sun angle ehanges. The sensor is relatively simple if the orbit is nearly eireular, so tnat the earth's angular subtense varies little in time, and if the semimajor axis equals a few earth radii. The determination of the loeal vertical when these two eonditions are not satisfied requires more sophistieated sensors. The diffieulty of this measurement permits one to state that the preeision of orbit determination from the satellite is at present essentially determined by the aeeuraey with whieh the loeal vertieal can be established. Several types of sun and star sensors have been used or proposed, the latter being potentially more aeeurate, but more eomplex than the former. Star sensors are generally used in a eontinuous tracking mode, rather than discontinuously on spinning satellites. The advantages of using star trackers are that the angular subtense of stars is much smaller than the sun's and that for all praetieal purposes they can be considered a true inertial referenee. The clock, a very aeeurate and stable oscillator, in gencral uses a temperature-eontrolled quartz crystal; long-term stability of one part in 10 million ean be obtained on today's satellites.

The planes of sight of both the earth and sun sensors are typieally perpendieular to the orbital plane, eontain the spin axis of the satellite, and form an angle δ. As the satellite spins, the sun and earth sensors deliver two trains of pulses which in general do not occur at the same time. llowever, for any given orbit, angular separation of the sensors, and position of the sun, there is one point P in orbit at whieh the pulse trains from the two sensors are in phase (Fig. 2). lf another sun sensor is used together with the earth sensor, at an angular separation δ', a seeond point P' ean be established in orbit. Alternatively, one eould use two earth sensors and one sun sensor. Thus each combination of three sensors is an orbital angle finder, which together with a elock can measure the time in whieh the satellite sweeps the known angle $P\hat{E}P'$. If the sun, rather than a star, is used as a reference, its angular motion relative to the orbit must be taken into aeeount. ln the case of an elliptic orbit, the argument (or angular coordinate) of the points P and P', relative to perigee, changes day by day beeause the projection of the sun line on the orbital plane moves with yearly period and beeause of perigee preeession. The orbital angle finder and the cloek, in measuring the time of flight of the satellite betwcen points in orbit, essentially measure the average angular veloeity of the satellite as it sweeps angles of known width.

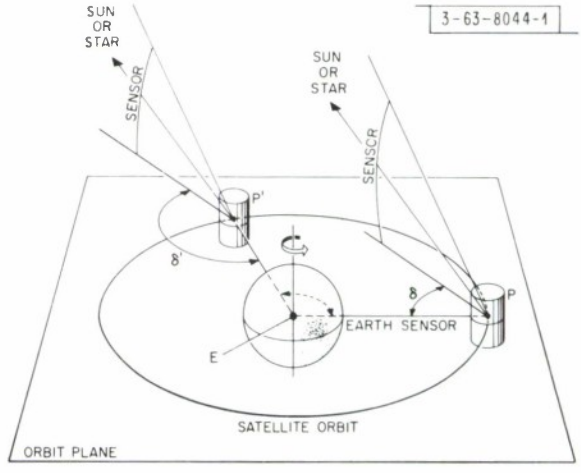

Fig. 2. Measurement af times af flight.

† It is well knawn that the arbital plane of an earth satellite is perturbed mainly by luni-salar effects and by the spherical harmanics in the geapatential. The magnitude af these perturbatians depends an the arbit cansidered.

Expanding the law of motion[26] in powers of the eccentricity ϵ,

$$\omega t = \Theta - \Theta_o - 2\epsilon\,[\sin(\Theta) - \sin(\Theta_o)] + \frac{3}{4}\,\epsilon^2\,[\sin(2\Theta) - \sin(2\Theta_o)] \quad , \qquad \text{(III-1)}$$

where Θ = satellite argument measured from perigee, ω = orbital radian frequency $\Theta = \Theta_o$ for $t = 0$.

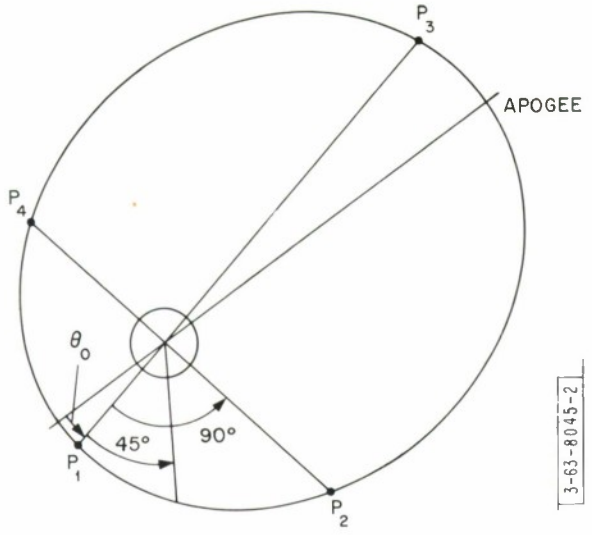

Fig. 3. Measurement points for orbit reconstruction.

Consider the times in which the satellite sweeps three consecutivc 90° sectors in orbit, defined by points P_1, P_2, P_3, and P_4 (Fig. 3), and let Θ_o be the argument at P_1. The satellite therefore moves from P_1 to P_2 in a time interval t_1 such that

$$\omega t_1 = \frac{\pi}{2} - 2\epsilon\,[\sin(\Theta_o + \frac{\pi}{2}) - \sin(\Theta_o)] + \frac{3}{4}\,\epsilon^2\,[\sin(2\Theta_o + \pi) - \sin(2\Theta_o)] \quad . \qquad \text{(III-2)}$$

Writing similarly the time intervals t_2, t_3 in which the satellite travels from P_2 to P_3 and P_3 to P_4, respectively, and taking linear combinations of the equations, one finds the (first-order) parameters:

$$\epsilon \sin(\Theta_o) = \frac{1}{4}\,[\omega(t_1 + t_2) - \pi] \quad , \qquad \text{(III-3)}$$

$$\epsilon \cos(\Theta_o) = \frac{1}{4}\,[\pi - \omega(t_2 + t_3)] \quad . \qquad \text{(III-4)}$$

The quantities ω, $\epsilon \sin(\Theta_o)$, $\epsilon \cos(\Theta_o)$ can be used as sufficient parameters, from which $\epsilon^2 \cos(2\Theta_o)$ can be determined. However, since this computation is not easily implemented, $\epsilon^2 \sin(2\Theta_o)$ are considered additional (second-order) parameters for the equation of motion; this is legitimate, since enough independent measurements of times of flight can be made.

To obtain the second-order parameters independently, the time t^* in which the satellite travels at 45° sector from P_1 to P' (Fig. 3) is measured, being

$$\omega t^* = \frac{\pi}{4} - 2\epsilon\,[\sin(\Theta_o + \frac{\pi}{4}) - \sin(\Theta_o)] - \frac{3}{4}\,\epsilon^2\,[\cos(2\Theta_o) - \sin(2\Theta_o)] \quad . \qquad \text{(III-5)}$$

Using this result and the previous equations, after some simplifications, the reconstruction of the law of motion in terms of these measurements is

$$\frac{\Theta - \Theta_o}{\omega} - t = \frac{1}{2}\left[\frac{T}{2} - (t_2 + t_3)\right]\sin(\omega t) + \frac{1}{2}\left[(t_1 + t_2) - \frac{T}{2}\right]\cdot\left[\cos(\omega t) - 1\right]$$

$$+ \frac{5}{3}\left[\frac{3 - 2^{\frac{1}{2}}}{4}\, t_1 + \frac{1}{2}\, t_2 + \frac{1 + 2^{\frac{1}{2}}}{4}\, t_3 - t^* - \frac{T}{4}\right]\cdot \sin(2\omega t)$$

$$+ \frac{5}{12}\left[\frac{T}{2} - (t_1 + t_3)\right]\left[\cos(2\omega t) - 1\right] \qquad \text{(III-6)}$$

to third order in ϵ. This expression involves only weighed sums and differences of the times of flight, as coefficients of the harmonic terms.

Some simple properties of the second-order reconstruction of the orbit are of practical interest because satellites are often placed in circular orbits around the principal body. Returning to (III-2) and dropping the terms in ϵ^2,

$$\epsilon \sin(\Theta_o) = \frac{1}{4}\,\omega(t_2 - t_3) \quad ; \quad \epsilon \cos(\Theta_o) = \frac{1}{4}\,\omega(t_1 - t_2) \quad , \qquad \text{(III-7)}$$

which are more compact forms of (III-3) and (III-4) for the second-order case. These expressions can be used to rewrite (III-6) for this case. The orbit reconstruction is now particularly simple, being

$$\frac{\Theta - \Theta_o}{\omega} - t = \frac{1}{2}\,(t_1 - t_2)\sin(\omega t) + \frac{1}{2}\,(t_3 - t_2)\left[1 - \cos(\omega t)\right] \quad . \qquad \text{(III-8)}$$

An interesting second-order property is that the times t', t'' in which the satellite sweeps any two angles, both of width $\Delta\Theta$ and opposed with respect to the focus are, to second order in ϵ,

$$\omega t' = \Delta\Theta - 2\epsilon\left[\sin(\Theta_o + \Delta\Theta) - \sin(\Theta_o)\right] \quad , \qquad \text{(III-9)}$$

$$\omega t'' = \Delta\Theta + 2\epsilon\left[\sin(\Theta_o + \Delta\Theta) - \sin(\Theta_o)\right] \quad , \qquad \text{(III-10)}$$

and, therefore,

$$T = \pi\,(t' + t'')/\Delta\Theta \quad . \qquad \text{(III-11)}$$

This equation provides alternate ways of measuring the period for quasi-circular orbits and is particularly simple if $\Delta\Theta$ is an integer fraction of a revolution. To second order in ϵ, clearly it is also

$$\omega = \frac{1}{2}\,(\omega' + \omega'') \quad , \qquad \text{(III-12)}$$

where ω' and ω'' are instantaneous angular velocities at two points in orbit opposed with respect to the focus.

As has been seen, the initial condition on the orbit is established by observing the time of coincidence of the outputs of a sun or star sensor and an earth sensor. If the sun is used as a reference, the on-board clock must be a solar clock, i.e., it must keep into account the variation of the transit time of the sun over a meridian of the satellite. If the orbital reconstruction is done on a day-by-day basis, it is sufficient for some applications to consider the mean sun motion; thus, one can use a constant-speed clock and correct for the mean sun motion either in carrying out the computation or by altering the angular distance of the sensors on the satellite by an appropriate amount. If, on the other hand, the initial conditions in each orbit must be accurately known for several years (e.g., for stationkeeping), it is necessary to use a true solar clock,

which can be implemented electronically. When the satellite spins about an axis which is not parallel to the earth's, the satellite's true solar time differs from the earth's (see Appendix A).

In determining the initial conditions on elliptic orbits for many consecutive days, one must consider the motion of the line apsides, which causes the point of coincidence between sensor outputs to move day by day along the orbit. Furthermore, if the sun is used as a reference, the point of coincidence moves with the projection of the sun line along the orbit. Thus, if the time coincidence occurs at point P^1 on the first orbit, it occurs at $P^2, P^3, \ldots P^n$ on successive orbits. Then, the n-th coincidence will occur at a time

$$t_n = nT + \Delta t\,(\varphi_n, \Theta_o) \quad .$$

Even though a true solar time is used, the fact that the angle φ_n is traveled on an elliptic orbit is cause of a measurement error. The error varies as

$$\delta = 2\epsilon \sin(\varphi_n)\ (\text{rad})$$

to second order in ϵ.

If the measurement is continued for a year or more, so that φ_n varies from 0 to 2π, the peak-to-peak error is $\delta_{p\text{-}p} \cong 228\,\epsilon$ (deg).

A simple way of eliminating this measurement error to second order in ϵ is then to repeat the determination of the initial condition twice per orbit at two points 180° apart and to take the arithmetic average of the two determinations.† This technique should be employed also when a star tracker is used in the orbital goniometer to eliminate the effect of apsidal line motion.

B. Application to Automatic Orbit Circularization

As an application of these ideas, we shall describe a system that would automatically reduce ϵ.‡ The controller is of the null-seeking type, requires little computation on the satellite, and

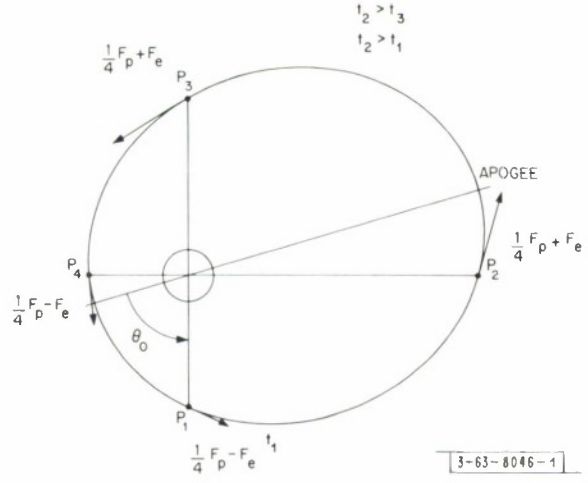

Fig. 4. Automatic circularization technique.

does not interact with the control of the satellite daily longitude. The orbital position is measured at points P_1, P_2, P_3, P_4, 90° apart (Fig. 4), with a system of angle-finders of the type which has been described previously. Let t_1, t_2, t_3, and t_4 be the times in which the satellite

† U.S. Patent Application 643493, filed 5 June 1967.

‡ This system has not been implemented on LES-6.

moves along four consecutive 90° sectors. Instead of computing the argument of apogee, the quadrant in which apogee is located with respect to the measured positions can be determined by noting that when $t_h = \max t_i$ $(i = 1, 2, 3, 4)$, apogee is between P_h and P_{h+1}, with the convention that $h + 1 = 1$ for $h = 4$. In the boundary case, $t_1 > t_2 = t_3$, apogee is at P_1, and similar relations hold when apogee is at P_2, P_3, and P_4. Thus, the position of apogee is determined qualitatively without computations, using only comparisons of times of flight.

The longitude (stationkeeping) control thrust is applied symmetrically about the orbital focus so that the eeeentricity is not modified.† For eonvenienee, if F_p is the impulsive stationkeeping eontrol thrust along the orbit tangent, $1/4\ F_p$ shall be applied four times per orbit, at points P_1 through P_4. To change the orbital eccentricity without affeeting the satellite period, the net tangential force applied during one orbit must be zero. A eontrol aetion $+F_e$ is applied, at eaeh of the two fix points which encompass apogee, followed by an action $-F_e$ at the two points encompassing perigee. This system of forces $\pm F_e$ tends to circularize the orbit and does not modify the satellite period.[23] In the boundary eases, the control aetion is modified simply. The time comparisons are repeated, and the corrective action $\pm F_e$ is applied until $t_i = t_h$ $(i, h = 1, 2, 3, 4)$, within the limits of aeeuracy of the sensors. F_e can be designed to satisfy fuel constraints or other requirements. If the stationkeeping corrections F_p and the circularizing eorreetion $\pm F_e$ are superimposed, the system of forces shown in Fig. 4 results.

To determine the preeision of this technique, the differenees between times of flight are written to second order in ϵ

$$\omega\,|t_1 - t_2| = 4\epsilon\,|\cos(\Theta_o)|\quad ,$$

$$\omega\,|t_2 - t_3| = 4\epsilon\,|\sin(\Theta_o)|\quad . \tag{III-13}$$

The control system operates to reduce the measured differences to zero, or

$$\omega(t_1 - t_2) + \sigma_1 - \sigma_2 = 0\quad ,$$

$$\omega(t_2 - t_3) + \sigma_2 - \sigma_3 = 0\quad , \tag{III-14}$$

where σ_i is the angular error made in measuring the corresponding 90° sector.

If σ_i is further written as

$$\sigma_i = \sigma_i^R + \sigma^S\quad ,\quad i = 0, 1, 2\quad ,$$

i.e., as the sum of a zero-mean and a systematic component, it follows that this control technique is insensitive to systematic angle errors. It is interesting to see what ϵ_r one would have from a constant measurement error $\sigma_1 - \sigma_2 = \sigma_2 - \sigma_3 = \sigma$. Then from (III-14),

$$\sigma = 4\epsilon_r\,|\cos(\Theta_o)|\quad ,\quad \sigma = 4\epsilon_r\,|\sin(\Theta_o)|$$

(in rad), or

$$\epsilon_r = \sigma/8^{\frac{1}{2}}\quad .$$

† This statement is proved in Sec. IV.

IV. OBSERVABILITY AND CONTROLLABILITY OF NEAR-CIRCULAR ORBITS

In this section, the dynamic problem of perturbations of near-circular orbits is discussed from the point of view of modern control theory. The problem of observability and controllability has been studied by several authors independently.[27-29] R. Brockett's results are the most complete and are used in parts A and B of this section. In part C, we discuss the meaning of the loss of controllability which occurs when the orbit equations are sampled once per day. We show that the symmetric thrusting policy which was discussed in Sec. III does not change the orbital eccentricity. This, together with a constraint which is shown to exist between the uncontrolled variables, permits us to show that this thrust policy leads to a Liapunov-stable system (i.e., one in which the uncontrolled variables cannot exceed a bound, which is proportional to the initial eccentricity). Thus we prove the feasibility of controlling the satellite longitude using observations appropriately made once per orbital period, and reconcile the classical approach presented in Secs. II and III and the point of view of modern control theory.

A. The Continuous Case

Let us consider the orbit equations in the case in which a small acceleration $\underline{u}$ is imparted to the satellite by on-board thrusters. If we call u_1, u_2, u_3 the three components along the dynamic coordinates r, $r_o\lambda$, $r_o\Theta$, the linearized equations of motion [(II-8), (II-9), (II-10)] become

$$\begin{cases} \ddot{r}_\delta - 3\omega^2 r_\delta - 2r_o\omega\dot{\lambda}_\delta = u_1 \quad , & \text{(IV-1)} \\ r_o\ddot{\lambda}_\delta + 2\omega_o\dot{r}_\delta = u_2 \quad , & \text{(IV-2)} \\ r_o\ddot{\Theta}_\delta + r_o\omega^2\Theta_\delta = u_3 \quad , & \text{(IV-3)} \end{cases}$$

where we have considered the spherical components of the earth's potential only, since we can superimpose the perturbations as long as the linearized equations hold.

Taking as variables $x_1 = r_\delta$, $x_2 = \dot{r}_\delta$, $x_3 = r_o\lambda_\delta$, $x_4 = r_o\dot{\lambda}_\delta$, $x_5 = r_o\Theta_\delta$, $x_6 = r_o\dot{\Theta}_\delta$, the matrix form of the resulting differential equation is

$$\dot{\underline{x}}(t) = \underline{A}\underline{x}(t) + \underline{B}\underline{u} \qquad \text{(IV-4)}$$

with

$$\underline{A} = \begin{bmatrix} 0 & 1 & 0 & 0 & 0 & 0 \\ 3\omega^2 & 0 & 0 & 2\omega & 0 & 0 \\ 0 & 0 & 0 & 1 & 0 & 0 \\ 0 & -2\omega & 0 & 0 & 0 & 0 \\ 0 & 0 & 0 & 0 & 0 & 1 \\ 0 & 0 & 0 & 0 & -\omega^2 & 0 \end{bmatrix} \qquad \text{(IV-5)}$$

and

$$\underline{B} = \begin{bmatrix} 0 & 0 & 0 \\ 1 & 0 & 0 \\ 0 & 0 & 0 \\ 0 & 1 & 0 \\ 0 & 0 & 0 \\ 0 & 0 & 1 \end{bmatrix} \tag{IV-6}$$

One can solve the equation by Laplace transformation and find with easy steps:

$$\begin{bmatrix} X_1 \\ X_3 \\ X_5 \end{bmatrix} = \begin{bmatrix} \frac{1}{s^2+\omega^2} & \frac{2\omega}{s(s^2+\omega^2)} & 0 \\ \frac{-2\omega}{s(s^2+\omega^2)} & \frac{s^2-3\omega^2}{s^2(s^2+\omega^2)} & 0 \\ 0 & 0 & \frac{1}{s^2+\omega^2} \end{bmatrix} \begin{bmatrix} U_1 \\ U_2 \\ U_3 \end{bmatrix} \tag{IV-7}$$

The natural response of Eq. (IV-4) with initial values $\underline{x}(0)$ is given, in the time domain, by

$$\underline{x}(t) = e^{\underline{A}t}\underline{x}(0) \quad , \tag{IV-8}$$

where $e^{\underline{K}t}$ is a $n \times n$ matrix,

$$e^{\underline{A}t} = L^{-1}(\underline{I}s - \underline{A})^{-1} = \frac{1}{2\pi j}\int_{\Gamma} (\underline{I}s - \underline{A})^{-1} e^{st}\, ds \quad , \tag{IV-9}$$

$\underline{I}$ being the identity matrix and Γ a contour enclosing all the eigenvalues of $(\underline{I}s - \underline{A})$. After some straightforward but lengthy calculations one obtains

$$e^{\underline{A}t} = \begin{bmatrix} 4-3\cos\omega & \frac{\sin\omega t}{\omega} & 0 & \frac{2(1-\cos\omega t)}{\omega} & 0 & 0 \\ 3\omega\sin\omega t & \cos\omega t & 0 & 2\sin\omega t & 0 & 0 \\ 6(-\omega t+\sin\omega t) & \frac{-2(1-\cos\omega t)}{\omega} & 1 & \frac{(-3\omega t+4\sin\omega t)}{\omega} & 0 & 0 \\ 6\omega(-1+\cos\omega t) & -2\sin\omega t & 0 & (-3+4\cos\omega t) & 0 & 0 \\ 0 & 0 & 0 & 0 & \cos\omega t & \frac{(\sin\omega t)}{\omega} \\ 0 & 0 & 0 & 0 & -\omega\sin\omega t & \cos\omega t \end{bmatrix} \tag{IV-10}$$

The solution of the foreed equation

$$\dot{\underline{x}}(t) = \underline{A}\underline{x}(t) + \underline{B}\underline{u}(t) \tag{IV-11}$$

is given by

$$\underline{x}(t) = e^{\underline{A}(t)}\underline{x}(0) + \int_0^t e^{\underline{A}(t-\sigma)}\,\underline{B}\underline{u}(\sigma)\,d\sigma \quad . \tag{IV-12}$$

Let us consider now the observability of the linearized, near-eireular equations of motion in the eontinuous ease. Since the last two equations in (IV-4) are deeoupled from the others, we can treat them separately.

As is well known, we must determine the rank of the matrix

$$\underline{L} = (\underline{C}, \underline{C}\underline{A}, \ldots, \underline{C}\underline{A}^{n-1})$$

whose rows are the rows of $\underline{C}$, $\underline{C}\underline{A}$, ete., where $\underline{C}\,\underline{x}$ is the observed vector. If we observe the radius x_1 only,

$$\underline{C}_1 = (1, 0, 0, 0) \quad ,$$

and

$$\underline{L}_1 = \begin{bmatrix} 1 & 0 & 0 & 0 \\ 0 & 1 & 0 & 0 \\ 3\omega^2 & 0 & 0 & 2\omega \\ 0 & -\omega^2 & 0 & 0 \end{bmatrix} \tag{IV-13}$$

Since rank $[L_1] = 3$ and the state vector $\underline{x}$ is of dimension 4, the system is not observable by measuring radius (or its derivative) only.

Now consider looking at the Θ dependent variable x_3. Here we have

$$\underline{C}_2 = (0, 0, 1, 0) \quad ,$$

and

$$\underline{L}_3 = \begin{bmatrix} 0 & 0 & 1 & 0 \\ 0 & 0 & 0 & 1 \\ 0 & -2\omega & 0 & 0 \\ -6\omega^3 & 0 & 0 & -4\omega^3 \end{bmatrix} \tag{IV-14}$$

This matrix is of rank 4 so the system is observable from x_3.

For the last equation we have

$$L_5 = \begin{bmatrix} 1 & 0 \\ 0 & 1 \end{bmatrix} \tag{IV-15}$$

which is nonsingular and therefore ensures the observability of x_5 and x_6.

Let us now consider the controllability of the system described by Eq. (IV-4), which is decided by considering the matrix

$$\underline{K} = (\underline{B}, \underline{A}\underline{B}, \ldots, \underline{A}^{n-1}\underline{B}) \quad .$$

If we control from u_1 (radial thrust alone),

$$\underline{K}_1 = \begin{bmatrix} 0 & 1 & 0 & -\omega^2 \\ 1 & 0 & -\omega^2 & 0 \\ 0 & 0 & -2\omega & 0 \\ 0 & -2\omega & 0 & 2\omega^3 \end{bmatrix} \tag{IV-16}$$

Since the rank of this matrix is only 3, control from u_1 is not possible.

In the case where u_1 is zero and u_2 is the control, the $\underline{K}$ matrix takes the form

$$\underline{K}_2 = \begin{bmatrix} 0 & 0 & 2\omega & 0 \\ 0 & 2\omega & 0 & -2\omega^3 \\ 0 & 1 & 0 & -4\omega^2 \\ 1 & 0 & -4\omega^2 & 0 \end{bmatrix} \tag{IV-17}$$

This matrix is of rank 4 and hence the system is controllable from u_2 alone. Thus we see that if only one thrust component is to be used it should be tangential to the orbit.

For the last two equations we have

$$\underline{K}_3 = \begin{bmatrix} 0 & 1 \\ 1 & 0 \end{bmatrix} \tag{IV-18}$$

which is clearly nonsingular. Hence u_3 can control the out-of-plane motion.

B. The Sampled Case

As we have seen in Sec. III, simple combinations of sensors permit us to establish points, or fixes, in the orbit. Thus we are interested in examining what happens to the orbit equations when they are sampled once, twice, and four times per orbit. We also assume that the control $\underline{u}$ is

applied only at the sampling times. Then $\underline{u}(kT)$ is the magnitude of the impulse applied at (kT). Thus the system is deserибed by the difference equation [from (IV-12)],

$$\underline{x}(kT + T) = e^{\underline{A}(T)}\underline{x}(kT) + e^{\underline{A}(T)}\underline{B}\underline{u}(kT) \quad , \tag{IV-19}$$

where T = sampling period = $2\pi/k\omega$, (k = 1, 2, 4). The transition matrices for the various eases are easily obtained from the expression of $e^{\underline{A}(t)}$ (IV-10). These are:

i. For $T = 2\pi/\omega$:

$$\begin{bmatrix} x_1 \\ x_2 \\ x_3 \\ x_4 \\ x_5 \\ x_6 \end{bmatrix}(Tk+T) = \begin{bmatrix} 1 & 0 & 0 & 0 & 0 & 0 \\ 0 & 1 & 0 & 0 & 0 & 0 \\ -12\pi & 0 & 1 & \frac{-6\pi}{\omega} & 0 & 0 \\ 0 & 0 & 0 & 1 & 0 & 0 \\ 0 & 0 & 0 & 0 & 1 & 0 \\ 0 & 0 & 0 & 0 & 0 & 1 \end{bmatrix}\begin{bmatrix} x_1 \\ x_2 \\ x_3 \\ x_4 \\ x_5 \\ x_6 \end{bmatrix}(kT) + \begin{bmatrix} 0 & 0 & 0 \\ 1 & 0 & 0 \\ 0 & \frac{-6\pi}{\omega} & 0 \\ 0 & 1 & 0 \\ 0 & 0 & 0 \\ 0 & 0 & 1 \end{bmatrix}\begin{bmatrix} u_1 \\ u_2 \\ u_3 \end{bmatrix}(kT) \tag{IV-20}$$

ii. For $T = \pi/\omega$:

$$\begin{bmatrix} x_1 \\ x_2 \\ x_3 \\ x_4 \\ x_5 \\ x_6 \end{bmatrix}(kT+T) = \begin{bmatrix} 7 & 0 & 0 & \frac{4}{\omega} & 0 & 0 \\ 0 & -1 & 0 & 0 & 0 & 0 \\ -6\pi & \frac{-4}{\omega} & 1 & \frac{-3\pi}{\omega} & 0 & 0 \\ -12\omega & 0 & 0 & -7 & 0 & 0 \\ 0 & 0 & 0 & 0 & -1 & 0 \\ 0 & 0 & 0 & 0 & 0 & -1 \end{bmatrix}\begin{bmatrix} x_1 \\ x_2 \\ x_3 \\ x_4 \\ x_5 \\ x_6 \end{bmatrix}(kT) + \begin{bmatrix} 0 & \frac{4}{\omega} & 0 \\ -1 & 0 & 0 \\ \frac{-4}{\omega} & \frac{-3\pi}{\omega} & 0 \\ 0 & -7 & 0 \\ 0 & 0 & 0 \\ 0 & 0 & -1 \end{bmatrix}\begin{bmatrix} u_1 \\ u_2 \\ u_3 \end{bmatrix}(kT) \tag{IV-21}$$

iii. For $T = \pi/2\omega$:

$$\begin{bmatrix} x_1 \\ x_2 \\ x_3 \\ x_4 \\ x_5 \\ x_6 \end{bmatrix}(kT+T) = \begin{bmatrix} 4 & \frac{1}{\omega} & 0 & \frac{2}{\omega} & 0 & 0 \\ 3\omega & 0 & 0 & 2 & 0 & 0 \\ -3\pi+6 & \frac{-2}{\omega} & 1 & \frac{(-3\pi+8)}{2\omega} & 0 & 0 \\ -6\omega & -2 & 0 & -3 & 0 & 0 \\ 0 & 0 & 0 & 0 & 0 & \frac{1}{\omega} \\ 0 & 0 & 0 & 0 & -\omega & 0 \end{bmatrix}\begin{bmatrix} x_1 \\ x_2 \\ x_3 \\ x_4 \\ x_5 \\ x_6 \end{bmatrix}x(kT) + \begin{bmatrix} \frac{1}{\omega} & \frac{2}{\omega} & 0 \\ 0 & 2 & 0 \\ \frac{-2}{\omega} & \frac{(-3\pi+8)}{2\omega} & 0 \\ -2 & -3 & 0 \\ 0 & 0 & \frac{1}{\omega} \\ 0 & 0 & 0 \end{bmatrix}u(kT) \tag{IV-22}$$

The z-transform of the responses can be obtained from these transfer matrices. Alternatively, one can start from the Laplace transfer function (IV-7), and find its z-transform for the appropriate value of T.

Using a tilda to indicate z-transform functions, one obtains easily:

i. For $T = 2\pi/\omega$:

$$\begin{bmatrix} \tilde{x}_1 \\ \tilde{x}_3 \\ \tilde{x}_5 \end{bmatrix} = \begin{bmatrix} 0 & 0 & 0 \\ 0 & \dfrac{+6\pi z}{\omega(z-1)^2} & 0 \\ 0 & 0 & 0 \end{bmatrix} \begin{bmatrix} \tilde{u}_1 \\ \tilde{u}_2 \\ \tilde{u}_3 \end{bmatrix} \tag{IV-23}$$

ii. For $T = \pi/\omega$:

$$\begin{bmatrix} \tilde{y}_1 \\ \tilde{y}_2 \\ \tilde{y}_3 \end{bmatrix} = \begin{bmatrix} 0 & \dfrac{4z}{\omega(z^2-1)} & 0 \\ \dfrac{-4z}{\omega(z^2-1)} & \dfrac{+3\pi z}{\omega(z-1)^2} & 0 \\ 0 & 0 & 0 \end{bmatrix} \begin{bmatrix} \tilde{u}_1 \\ \tilde{u}_2 \\ \tilde{u}_3 \end{bmatrix} \tag{IV-24}$$

iii. For $T = \pi/2\omega$:

$$\begin{bmatrix} \tilde{y}_1 \\ \tilde{y}_2 \\ \tilde{y}_3 \end{bmatrix} = \begin{bmatrix} \dfrac{z/\omega}{z^2+1} & \dfrac{2}{\omega}\dfrac{z(z+1)}{(z-1)(z^2+1)} & 0 \\ \dfrac{-2z(z+1)}{\omega(z-1)(z^2+1)} & \dfrac{z[(8-3\pi)z^2-16z+(8-3\pi)]}{2\omega(z^2+1)(z^2-1)} & 0 \\ 0 & 0 & \dfrac{z/\omega}{(z^2+1)} \end{bmatrix} \begin{bmatrix} \tilde{u}_1 \\ \tilde{u}_2 \\ \tilde{u}_3 \end{bmatrix} \tag{IV-25}$$

The test for observability and controllability is of the same form as for the continuous case. However, the $\underline{A}$ and $\underline{B}$ matrices must be replaced by the matrices in Eqs. (IV-20), (IV-21), (IV-22) for the different cases. The results of the calculations are given in Appendix B and summarized in Table I.

It is interesting to note at this point that the techniques of orbit reconstruction discussed in Sec. III satisfy the observability test. The flight times between points in orbit depend both on radius and angle information, as is readily verified. Four measurements of times along the orbit are sufficient for complete observability.

Some recent work[30] has addressed itself to the problem of finding optimal solutions (in a least-square sense) to near-circular orbit control. For optimum control theory to be really

TABLE I

SUMMARY OF CONTROLLABILITY AND OBSERVABILITY PROPERTIES OF THE LINEARIZED ORBITAL EQUATIONS

	Meosurements per Orbit			Continuous Meosurement
	One	Two	Four	
Observing (in-plone)				
Rodiol observotions	No	No	No	No
Tongentiol observotions	No	No	Yes	Yes
Rodiol ond tongentiol	No	Yes	Yes	Yes
Control (in-plone)				
Rodiol thrust	No	No	No	No
Tongentiol thrust	No	No	Yes	Yes
Rodiol ond tongentiol	No	Yes	Yes	Yes
Observing (out-of-plone)				
Orbit normol observotion	No	No	Yes	Yes
Control (out-of-plone)				
Orbit normol thrust	No	No	Yes	Yes

useful, the system must be completely observable and controllable. Thus I. B. Chammas' study deals with the cases which are completely controllable and observable (see Table I). The cost function which is minimized is

$$q = \int_0^\sigma (\underline{u}'\underline{u} + \alpha \underline{y}'\underline{y})\, dt \quad ,$$

where $\underline{y}$ is a linear transformation of the measured vector $\underline{x}$. The author studies the cases in which (1) σ is finite and large and $\alpha = 0$, for which he finds a time-varying optimal control, and (2) $\sigma \to \infty$ and $\alpha \neq 0$, for which he finds a constant control law.

The optimal control laws depend on all components of the measurement vector $\underline{x}$. While the instrumentation presently available does not allow us to conveniently measure x_1 nor x_2, it is nonetheless instructive to consider the optimal control policies as performance bench-marks. Future study should also focus on performance criteria of the type

$$q = \int_0^\sigma (|\underline{u}| + \alpha \underline{y}'\underline{y})\, dt$$

and constraints of the type

$$\int_0^\sigma |\underline{u}|\, dt < L \quad .$$

C. Stable Control of the System with Daily Sampling

It is important now to examine the exact meaning of the lack of controllability of the dynamic equations in the case of one sampling per orbit. It is seen from (IV-23) that the longitudinal

coordinate x_3 is controllable, while x_1 is not. The question therefore arises as to whether it is possible for x_1 to grow without bound when x_3 only is controlled. Physically, this would correspond to the orbit becoming increasingly elliptical, while the orbit semimajor axis remains constant, as required by the fact that x_3 is controlled. We shall prove that the double thrusting policy which was introduced in Sec. III has the property that the orbital eccentricity remains constant and equal to its initial value.

From the z-transfer matrix (IV-23), the transfer function between x_3 (the longitudinal coordinate) and u_2 (tangential thrusting) is

$$\tilde{x}_3 = \frac{6\pi z}{\omega(z-1)^2}\,\tilde{u}_2 \quad , \tag{IV-26}$$

which corresponds to a double integrator. Thus $\tilde{x}_3$ is controllable. But controllability of the longitudinal coordinate sampled once per day means that $\tilde{x}_3$ can be driven to zero. This in turn implies that the orbital period and therefore, by Kepler's third law, the semimajor axis of the orbit can be made constant.

It is easy to show that for linear expansions of the orbital motion the semimajor axis equals the average of the radius over one orbit.† Then the semimajor axis must be $\hat{x}_1 + r_o$ and an expression for the average over one orbit of x_1 is found from the transition equation [see (IV-10)],

$$x_1 = (4 - 3\cos\omega t)\,x_1(0) + \frac{1}{\omega}\sin\omega t\, x_2(0) + \frac{2}{\omega}(1-\cos\omega t)\,x_4(0) \quad , \tag{IV-27}$$

and thus

$$\hat{x}_1 = 4x_1(0) + \frac{2}{\omega}\,x_4(0) \quad . \tag{IV-28}$$

If we drive $\tilde{x}_3$ to zero, $\hat{x}_1$ must equal zero, so that the semimajor axis equals r_o. Then on successive samplings the uncontrolled coordinate x_1 is constrained by the equation

$$2\tilde{x}_1 + \frac{1}{\omega}\,\tilde{x}_4 = 0 \quad . \tag{IV-29}$$

Thus, as was expected on physical grounds, the values of $\tilde{x}_1$ and $\tilde{x}_4$ are not independent when x_3 is controlled to zero.

Consider now what happens if one samples x_1 so that its value equals $\hat{x}_1$. Then Eq. (IV-28) becomes

$$3\tilde{\hat{x}}_1 + \frac{2}{\omega}\,\tilde{x}_4 = 0 \quad , \tag{IV-30}$$

which is the relationship that was established in Sec. II when sampling was performed in such a manner as to eliminate the daily variation in r_δ and $\ddot{r}_\delta$ [see Eq. (II-19)].

In Sec. III we had established that the daily motion (eccentricity dependent) was eliminated if one observed once per orbit by taking the average of two observations at intervals π/ω. Also, it was claimed that splitting the thrust value (determined once per orbit) in two equal parts applied at π/ω intervals maintained the orbital eccentricity at a constant value. To check this, we use again the transition matrix (IV-10) and find immediately that the new observable

$$x'_3 = \frac{1}{2}\left[x_3(0) + x_3\left(\frac{\pi}{\omega}\right)\right] \tag{IV-31}$$

† In general, the semimajor axis differs from the time average of the radius taken during one orbit (see, for example, Ref. 26).

does not contain any orbit periodic eomponents. This new observable is thus the mean longitudinal position.

To find the effect of symmetric thrusting at π/ω intervals on the eccentrieity ϵ, we note that

$$\epsilon \simeq \frac{r_{max} - r_o}{r_o} = \frac{x_{1\ max}}{r_o} = -\frac{x_{1\ min}}{r_0} \quad . \tag{IV-32}$$

Thus for the eceentricity to be constant it must be $x_{1\ max}$ = constant.

From the transition matrix it is easily

$$x_{1\ max} = 4x_1(0) + \frac{2}{\omega}\ x_4(0) + \sqrt{\left[\frac{x_2(0)}{\omega}\right]^2 + \left[3x_1(0) + \frac{2}{\omega}\ x_4(0)\right]^2} \quad . \tag{IV-33}$$

Sinee we control x_3, it is because of (IV-29),

$$x_{1\ max} = \sqrt{\left[\frac{x_2(0)}{\omega}\right]^2 + \left[3x_1(0) + \frac{2}{\omega}\ x_4(0)\right]^2} \quad . \tag{IV-34}$$

From the sampled equations for $T = \pi/\omega$ (IV-20) used with the constraint $u_2(kT + T) = u_2(kT)$ for k even, one has easily

$$\begin{bmatrix} x_1 \\ x_2 \\ x_4 \end{bmatrix} (kT + 2T) = \begin{bmatrix} 1 & 0 & 0 \\ 0 & 1 & 0 \\ 0 & 0 & 1 \end{bmatrix} \begin{bmatrix} x_1 \\ x_2 \\ x_4 \end{bmatrix} (kT) + \begin{bmatrix} \frac{4}{\omega} \\ 0 \\ -6 \end{bmatrix} u_2(kT) \tag{IV-35}$$

which yields

$$x_2(kT + 2T) = x_2(kT) \quad , \tag{IV-36}$$

and

$$x_1(kT + 2T) = x_1(kT) + \frac{4}{\omega}\ u_2(kT) \quad , \tag{IV-37}$$

$$x_4(kT + 2T) = x_4(kT) - 6\ u_2(kT) \quad . \tag{IV-38}$$

Since x_2 remains unchanged and so does the quantity

$$3x_1 + \frac{2}{\omega}\ x_4 \text{ (from the last two equations),}$$

the eecentrieity remains unchanged beeause of (IV-32) and (IV-34). Thus we have shown that, when x_3 is controlled by thrusting equally at points 180° apart in orbit, the eecentricity is not changed. Using the eceentricity as a parameter, if the sampling is done so that $x_2 = 0$, one has from (IV-34), (IV-32), and (IV-29),

$$\tilde{x}_1 = -\epsilon\ r_o \quad , \tag{IV-39}$$

$$\tilde{x}_4 = 2\ \omega\ \epsilon\ r_o \quad , \tag{IV-40}$$

for this control poliey.

To conclude, we have shown how it is possible to control the longitudinal motion of the satellite by sampling once per orbit. The radius is uncontrollable, but constrained to the value of the longitudinal drift rate by Eq. (IV-29). Equation (II-9), established for an appropriate value of the sampling phase, was found again to be valid. It was shown how it is possible to ensure that the eccentricity remain constant and thus that $x_1(t)$ and $x_2(t)$ be bounded, $\tilde{x}_1 = -\epsilon r_o$, and $\tilde{x}_4 = 2\omega\epsilon r_o$.

V. ANALYSIS AND DESIGN OF A FINITE-STATE CONTROLLER

A. Preliminaries

Section V describes the design of the controller which was actually flown in LES-6. The design is based on the assumption that only satellite angular position can be measured with the instrumentation available. At the time of this design, it was assumed that daily angular drifts of fractions of a degree per day could not be measured in practice. A preliminary estimate of sensor errors, solar clock errors, and the coupling of orientation errors into position errors led to the conclusion that satellite position would not be measured more accurately than about 2 degrees peak-to-peak over long periods of time, with an rms value of 1.3 degrees. It was thus established that longitude would be measured in a quantized manner and the smallest quantization window was set at 2 degrees.

It was also decided, on the basis of the analysis of Secs. III and IV, that we would sample once per day and observe only the mean daily longitudinal position. Further, it was decided that the daily observation would consist of the average of two observations made at opposite points in orbit (with respect to the earth center), to decouple the observation from the daily (eccentricity dependent) motion. Finally, it was decided to thrust symmetrically with respect to the earth center, so that eccentricity, although not controlled, would not increase, as discussed in Sec. IV (see Fig. 5).

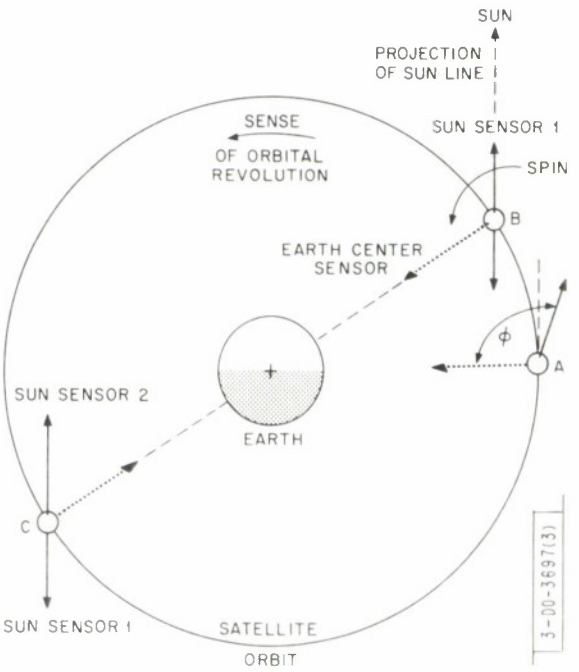

Fig. 5. Meosurement of sotellite position on LES-6.

Since drift velocity was not directly measurable, damping of the motion could be achieved by observing the transitions of the satellite into adjacent two-degree-wide longitude bands. This suggested a finite-state machine realization of the controller.

The thrusters available on the satellite are of two types: cold-gas thrusters and pulsed plasma thrusters. The gas thrusters provide a linear acceleration of about 0.35×10^{-5} m/sec^2 and the plasma thrusters about 0.95×10^{-7} m/sec^2.† These figures are to be compared to the linear acceleration caused by the earth's equatorial ellipticity which is at most 0.545×10^{-7} m/sec^2. Thus it was decided that the plasma thrusters would be used only for steady-state tracking, since their maximum effect (in continuous operation) is only about twice the disturbing acceleration at

† Both figures keep into account the duty-cycle of operation of the system.

the worst earth longitude. The need to operate with two widely different thrusters posed an additional constraint on the design of the controller. The gas thruster system was, however, considered the primary system, since there has been no previous flight experience with the plasma thrusters. As discussed in Sec. VIII, these were indeed extremely successful and have been used exclusively, up to the time of this writing, for steady-state station tracking.

The orbit control system of LES-6 has the following modes of operation:

Command Mode:– Either the gas or plasma thrusters can be operated on command from the ground. The earth direction and the firing angles (with respect to the orbit tangent) are determined by using on-board sensors. The thrusters shut off automatically after predetermined time intervals, which can be selected from the ground.

Automatic Mode:– Operation is completely self-contained with either thruster system. Two modes are available, with automatic switchover: (1) new station acquisition, and (2) station tracking, with self-contained damping of the relative motion.

In all modes, thrust is applied to the satellite in the direction of the orbit tangent, which for a circular orbit is normal to the satellite-earth line, determined by an earth sensor. Total impulses of different values are obtained by firing the thrusters for a fixed part of each of several rotations, the spin rate being measured by sun sensors.

The satellite position is determined using the combination of sun and earth sensors described in Sec. III. Sun sensors were preferred to star sensors because of their simplicity and ruggedness. The position of the satellite must then be compared with the position of the ground station at a given time. Since any earth meridian moves at a constant angular speed in space (disregarding small secular changes of earth rotation rate), an on-board clock can determine the position of a station of known longitude. The clock delivers a pulse every 12 hours: the time difference between a clock pulse and the sensor coincidence pulse is then a direct measurement of the longitude displacement. The fact that the satellite position is measured with respect to the sun projection on the orbit plane requires that the clock be a "true solar clock," which should indicate the transit time of the sun at the desired earth longitude (see Appendix A). This transit time (ephemeris) displacement is shown in Fig. 6 for the year 1969; secular changes can be disregarded for satellites having a lifetime of a few years. If the spin axis is normal to the orbit and the orbit is equatorial, the true solar time of the earth station can be compared directly with the position or coincidence pulse delivered by the sensor system. A high-precision oscillator and counter deliver a pulse every mean solar day, which is advanced or retarded electronically in accordance with the day of the year† (see Sec. VII). Alternatively, a "mean solar clock" can be used if the position of the satellite is measured with a special sun sensor‡ or a star tracker. Spin axis misalignment causes a position error, whose worst-case magnitude during a

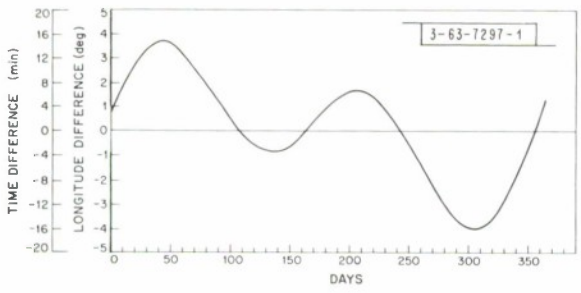

Fig. 6. Sun transit time displacement for 1969.

† For a satellite lifetime of 5 years, clock accuracy of about 1 part in 10^9 is necessary.

‡ U.S. Patent Application 643493, filed 5 June 1967.

year is ±0.55° of longitude per degree of misalignment for a satellite such as LES-6 (see Appendix A and Ref. 31).

Automatic acquisition of new stations, i.e., new earth longitudes, is based on the fact that the time of arrival of the daily pulse from the internal clock determines the stationkeeping longitude. If satellite position is measured at the 9 a.m. position in orbit (point B in Fig. 5), the control system maintains synchronism with that earth station whose true solar time is 9 a.m. at the time of arrival of the internal clock pulse. Therefore, new stations are selected automatically by changing the phase of the internal pulse, i.e., by resetting the clock with a command when the true solar time of the desired station is 9 a.m. Station changes could be completely automatic if the time of occurrence of the reset pulse were preprogrammed on the satellite.

After acquisition, the satellite can stationkeep at any geocentric longitude, which implies bidirectional control action, since the disturbing force changes sign in accordance with Eq. (II-36), and its motion is constrained to a band around the station, whose width is determined by the measurement accuracy. A sequential damping procedure, designed to use fuel with high efficiency, ensures the convergence to this band.

The most important performance parameters are fuel consumption (both in steady state and in damping), the settling time after acquisition, sensitivity to measurement errors, the time necessary to acquire a new station, and the number of possible station changes.

B. System Analysis (Ref. 32)

In this section we use the "weak-coupling" approximation that was established in Secs. III and IV. The relevant equations are repeated here, with the definition of constants necessary for the applications. Variables are sampled once per day, but the star notation is dropped for simplicity.

The geopotential perturbation is given by (II-36),

$$\ddot{\lambda}_G \simeq -1.54 \times 10^{-3} \sin 2(\lambda - \lambda_o) \text{ deg/day}^2 \quad , \tag{V-1}$$

where $\lambda_o \simeq 73°$ east longitude is the position of the minor axis of the geopotential ellipse. The change in radius is related to the angular drift velocity by (II-19),

$$\frac{r_\delta}{r_o} = -\frac{2}{3} \frac{\dot{\lambda}(\text{deg/day})}{360°} \quad , \tag{V-2}$$

where r_o = synchronous radius $\simeq 42{,}165$ km.

The effect of the thrusters is obtained by computing the total change in linear velocity per day Δv_d, knowing the thrust level, the mass of the satellite, and the time during which the thrusters operate. For small Δv_d, the daily angular acceleration caused by the thrusters is obtained from the laws of orbital motion,

$$\ddot{\lambda}_T = -3 \times 360° \frac{\Delta v_d}{v_o} \text{ (deg/day}^2\text{)} \quad , \tag{V-3}$$

where v_o = synchronous linear velocity $\simeq 3{,}300$ m/sec. The total angular acceleration is therefore

$$\ddot{\lambda} = \ddot{\lambda}_G + \ddot{\lambda}_T \quad . \tag{V-4}$$

A convenient approximate representation of the effect of the geopotential is obtained using a "potential energy function" V_e, dependent on the satellite longitude sampled once per day. By integration,

$$V_G(\lambda) = -\int_o^{\lambda} \ddot{\lambda}_G \, d\lambda = -4.4 \times 10^{-2} \cos 2(\lambda - \lambda_o) \text{ (deg/day)}^2 \quad , \qquad \text{(V-5)}$$

recalling the necessary transformation from radians to degrees. The thruster is designed to produce a very small change of orbital angular velocity per day. If the satellite drift per day remains small, firing the thruster every day for a fixed time results in a constant daily change of mean drift rate, i.e., a constant mean drift acceleration. If, furthermore, the firing time per orbit is made to depend only on the satellite mean daily longitude, the thruster-imparted acceleration is sensibly conservative, and a second "potential energy function" V_T can describe the longitude caused by the thruster. The satellite drift motion can therefore be studied in an approximate but expressive way with the aid of a "total potential energy function" in the mean relative satellite longitude λ measured once per day.

In the system discussed here, λ is quantized in steps of magnitude ΔL. The daily thruster impulse takes on two different values, I' between ΔL and $2\Delta L$ or $-\Delta L$ and $-2\Delta L$, and I'' elsewhere for $|\lambda| < L$. The direction of thrust is such as to cause the satellite to drift toward the station.† The resulting potential energy function is shown qualitatively in Fig. 7.

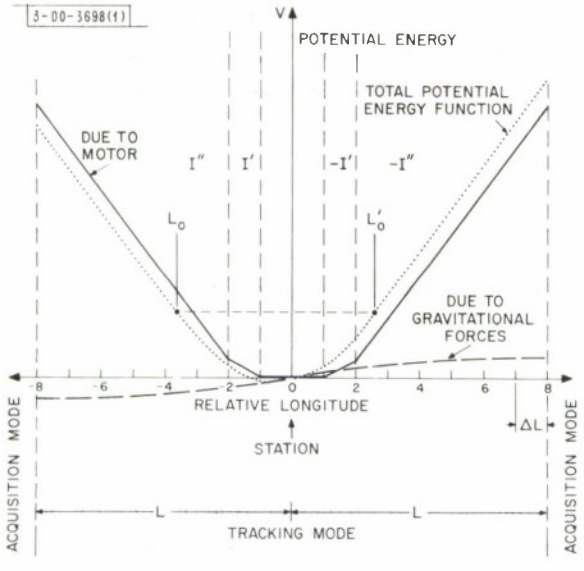

Fig. 7. Qualitative behavior of the potential energy function.

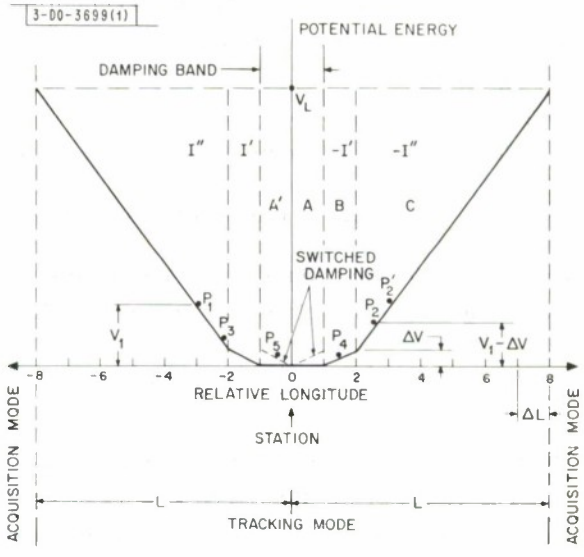

Fig. 8. Switched damping technique.

If, for example, the satellite were initially at L_o with no drift velocity, it would oscillate between L_o and L'_o. Damping is therefore necessary and is accomplished in "damping bands" A and A', ΔL wide about the station, as seen in Fig. 8. When the satellite is in A, a daily impulse is applied if the satellite has entered A by crossing the zero (station) line, and no impulse is applied if it has entered from B. A similar firing strategy is used when the satellite is in A'.

† Notice that an increase in instantaneous orbital velocity increases the semimajor axis and the period, thus actually slowing down the satellite with respect to the station.

Consider, as an example, the behavior of a satellite starting at P_1 with no drift velocity, assuming for simplicity that $V_e = 0$. The satellite would be accelerated by the thrusters and reach the station with kinetic energy (in the variable $\dot{\lambda}$) equal to V_1. No impulse would be applied in A', but upon entering A, a damping impulse would be called for once per day, so that in band A the kinetic energy of the satellite would decrease by ΔV (Fig. 8). Thus the satellite would only reach P_2 instead of P_2', invert its motion, and enter A from B. No impulse would therefore be applied until the satellite crossed from A to A'. In each complete oscillation, the energy decreases by $2\Delta V$ until the satellite remains in bands A or A'. As seen in the following, the damping impulse is changed adaptively to reduce the residual relative kinetic energy to very small values. I' and I'' are made large enough so that there is a potential energy minimum in a neighborhood of the station for any station longitude and a stable equilibrium point occurs within $\pm\Delta L$ from the station.

1. Station Acquisition Mode

The automatic system enters the station acquisition mode when its longitude differs from the station's by more than $\pm L$ degrees. L is made sufficiently large so that this event only occurs as a consequence of a station change. Redundancy techniques are used to avoid spurious transitions into the acquisition mode. The thruster immediately fires for a fixed length of time at opposite points of the orbit, causing the satellite to drift toward the station. When the desired geocentric longitude is reached, the satellite returns to near synchronous orbit by firing the thruster in the same manner in the opposite direction. Having completed the homing firing sequence, the system switches to the station-tracking mode. As a result of orbit perturbations during the transfer between stations, in general at the beginning of tracking mode operation the satellite has a residual drift velocity relative to the new station, which must be damped.

If $\dot{\lambda}_o$ is the drift rate impressed on the satellite at the beginning of the acquisition mode, then within the limits of approximation of (V-1) the energy conservation theorems in the variables $\dot{\lambda}$ and λ can be written as for a point mass whose motion were described by this equation. From (V-5) and Fig. 9, for acquisition of any station it must be $\frac{1}{2}\dot{\lambda}_o^2 \geq \Delta V_{G\,max} = 8.8 \times 10^{-2}$ (deg/day)^2, or $\dot{\lambda}_o \geq 0.42$ deg/day. Then let $\dot{\lambda}_o = 0.42\,k$ deg/day, where $k > 1$ is a coefficient which determines the acquisition speed. If the relative drift velocity imparted by the thrusters is i deg/day per sec of thruster operation, the thruster on-time for acquisition is $T_A = 0.42\,k/i$ sec. The drift velocity must vary by the same amount twice because there must be two equal and opposite impulses. If the fuel consumption is $\dot{m}_f$ gm/sec, the fuel required per station acquisition is $m_{f_A} = 0.84\,\dot{m}_f\,k/i$. Notice that the inequality $\dot{\lambda}_o^2/2 \geq \Delta V_{G\,max}$ need be satisfied only for transfers between the minor and the major axis of the earth's equator. One could compute on board the minimum value of the acquisition

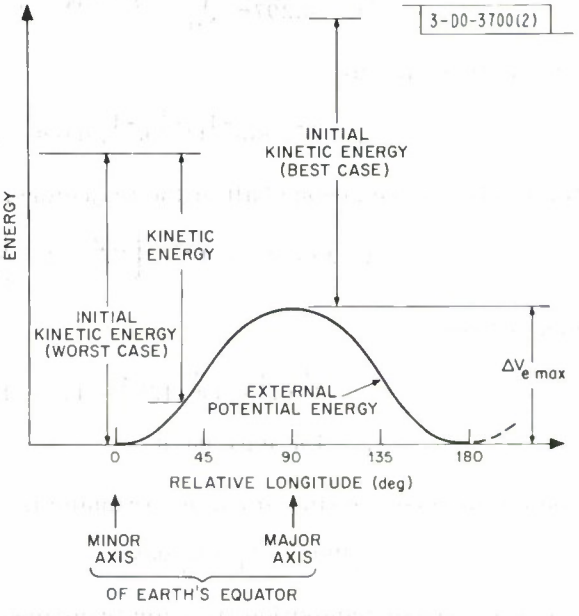

Fig. 9. Kinetic energy for the transfer between orbits.

impulse as a function of the required longitude displacement, using (V-5), and fire the thruster accordingly, if the additional complexity were justified.

The speed of station acquisition can be derived by integrating (V-1) with initial condition $\dot{\lambda} = \dot{\lambda}_o$ for various longitudes of the old and the new station. To obtain results in closed form, (V-5) can be approximated, dropping the phase term Θ_o, by

$$V_G(\lambda) \cong -4.4 \times 10^{-2} \left(1 - \frac{16}{\pi^2} \lambda^2\right) \text{ (deg/day)}^2 \tag{V-6}$$

for $-\pi/4 \leqslant \lambda \leqslant \pi/4$, where λ must be expressed in radians. This second-order approximation to $\cos 2\lambda$ is in error by 5 percent at $\lambda = \pi/8$. The worst case for a 90° transfer is clearly that in which the old station is on the minor axis of the earth's equatorial ellipse and the new station is on the major axis (Fig. 9). The initial kinetic energy becomes

$$V_o = 8.8 \times 10^{-2} k^2 \text{ (deg/day)}^2 \quad . \tag{V-7}$$

Defining $\xi \equiv 2k^2 - 16(\lambda^2/\pi^2)$, the kinetic energy during the first half of the trajectory is, referring to Fig. 9,

$$V_e(\Theta) = 4.4 \times 10^{-2} \xi \quad , \tag{V-8}$$

and therefore expressing the velocity in rad/day,

$$\dot{\lambda} = (0.297\pi/180)\, \xi^{\frac{1}{2}} \quad , \tag{V-9}$$

The time to travel an angle of 45° is then

$$t_1 = \frac{180}{0.297\pi} \int_o^{\pi/4} \xi^{-\frac{1}{2}}\, d\lambda \quad , \tag{V-10}$$

which integrates to

$$t_1 = 152 \sin^{-1}(2^{-\frac{1}{2}} k^{-1}) \text{ days} \quad . \tag{V-11}$$

Similarly, in the second half of the trajectory,

$$V_e(\lambda) = 4.4 \times 10^{-2} \left[2k^2 - 2 + \frac{16}{\pi^2} (\lambda - \frac{\pi}{2})^2\right] \quad , \tag{V-12}$$

and defining

$$\psi = 2^{\frac{1}{2}} (k^2 - 1)^{\frac{1}{2}} / [2k^2 - 1)^{\frac{1}{2}} - 1] \quad , \tag{V-13}$$

$$t_2 = 152 \log \psi \text{ days} \quad , \tag{V-14}$$

and the worst-case time for a 90° transfer is

$$t_w(90°) = t_1 + t_2 \text{ days} \quad . \tag{V-15}$$

The worst-case acquisition time for transfers smaller than 90° occurs when the new and the old station are located symmetrically with respect to the 45° longitude (Fig. 9) and can be calculated easily with the previous procedure. The acquisition time for 180° transfer between any two positions is clearly twice t_w (90°). The best-case 90° transfer occurs when the old station is on the major axis and the new station is on the minor axis.

2. Fuel Consumption in Steady State

The optimum steady-state condition, from the point of view of fuel consumption, would be one in which a constant acceleration were applied to the satellite to equal the tangential drift acceleration at the satellite geocentric longitude. This ideal situation cannot be achieved because perfect damping is not possible in practical controllers. As will be seen later, the damping impulse is reduced adaptively to a small value I_n during the damping maneuver. After the controller has reached the last value of I_n, either the impulse in A and A' of Fig. 8 is reduced to zero (first system), or the impulse remains at the value I_n but the switching is discontinued (second system).

a. First System

No impulse is applied in the damping band after damping has been completed. The potential configuration in this case is shown in Fig. 10. The longitude interval $4\Delta L$ is sufficiently small so that the external acceleration given by (V-1) can be considered constant. Impulses $+I'$ and $-I'$ are applied in opposite directions on the sides of the damping band. For a daily impulse I the

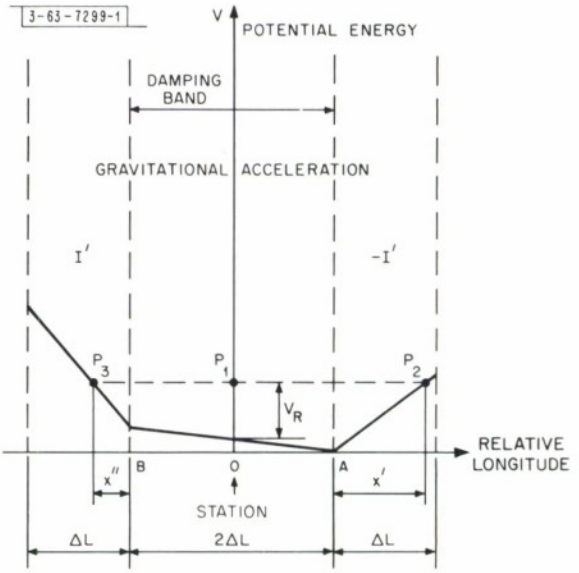

Fig. 10. Potential energy for the first system.

energy acquired by the satellite in traveling $\Delta\lambda$ degrees is $V = I\Delta\lambda\ (\text{deg/day})^2$. Let F_e be the maximum value of f_e and define $\alpha_n \equiv I_n/F_e$, and $\alpha' = I'/F_e$. Since the satellite must remain within $\pm\Delta L$ of the origin after damping, α' must be greater than one. At the end of the damping, the satellite has at most residual energy

$$V_R = (I_n + f_e)\,\Delta L \quad . \tag{V-16}$$

This worst-case situation occurs if the satellite reaches point B in Fig. 10 with zero velocity. If this does not occur, the satellite exits from the damping band and the damping cycle continues. In general, the satellite velocity will be zero at some point internal to the damping band, in which case the residual energy is smaller than V_R. The damping cycle ends at the origin, since the satellite longitude is measured in steps of width ΔL. The relative kinetic energy is zero at P_2, where the potential energy is, with the reference of Fig. 10,

$$V_c(P_2) = V_R + f_c \Delta L = (I_n + 2f_e)\Delta L \quad . \tag{V-17}$$

From simple geometrie eonsiderations, the position P_2 is defined by

$$x' = (I_n + 2f_e)\Delta L/(I' - f_e) \quad . \tag{V-18}$$

Elementary considerations on the equation of motion for a eonstant acceleration field yield that at time

$$t_A = (2x')^{\frac{1}{2}}/(I' - f_e) = \dot{\lambda}_A/(I' - f_e) \quad , \tag{V-19}$$

wherc $\dot{\lambda}_A$ is the drift velocity with which the satellite passes at A (Fig. 10),

$$\dot{\lambda}_A = [2(I_n + 2f_e)\Delta L]^{\frac{1}{2}} \quad . \tag{V-20}$$

The travel time between A and B is

$$t_{AB} = (\dot{\lambda}_A - \dot{\lambda}_B)/f_c \quad , \tag{V-21}$$

wherc

$$\dot{\lambda}_B = (2I_n \Delta L)^{\frac{1}{2}} \quad , \tag{V-22}$$

The velocity at P_3 is zero, and therefore

$$t_B = \dot{\lambda}_B/(I' - f_e) \quad . \tag{V-23}$$

Sinee this eycle repeats itself, thc fuel eonsumption per second is proportional to

$$Q^{(1)} = (t_A + t_B)/(t_A + t_{AB} + t_B) \quad . \tag{V-24}$$

By using (V-17), (V-18), (V-22), (V-24), and letting $\lambda - \lambda_o = \delta$ in (V-1), the expression for thc steady-state fuel consumption when stationkeeping at any position in orbit is obtained:

$$Q^{(1)} = \alpha' F_e \frac{\zeta_1 + \zeta_2}{\zeta_1 + \zeta_2 + \dfrac{(\alpha_n + 2|\sin 2\delta|)^{\frac{1}{2}} - \alpha_n^{\frac{1}{2}}}{|\sin 2\delta|}} \quad , \tag{V-25}$$

where $\zeta_1 = (\alpha_n + 2|\sin 2\delta|)^{\frac{1}{2}}/(\alpha' - |\sin 2\delta|)$ and $\zeta_2 = \alpha_n^{\frac{1}{2}}/(\alpha' + |\sin 2\delta|)$. By taking the limit for $\sin 2\delta \to 0$, thc steady-state fuel consumption for $f_e = 0$ is found:

$$Q_o^{(1)} = 2F_e\alpha_n/(1 + 2\alpha_n/\alpha') \quad . \tag{V-26}$$

b. Second System

Thc last damping impulse I_n is retained in the part of the damping band where it was last applied. The potential eonfiguration for this system is shown in Fig. 11. The residual energy is again given by (V-16). The same procedure used before yields the steady-state fuel consumption for this system:

$$Q^{(2)} = F_c \frac{\alpha'\zeta_1 + \alpha_n/\zeta_3}{\zeta_1 + \zeta_3^{-1} + \dfrac{(\alpha_n + 2|\sin 2\delta|)^{\frac{1}{2}} - \zeta_3}{|\sin 2\delta|}} \quad , \tag{V-27}$$

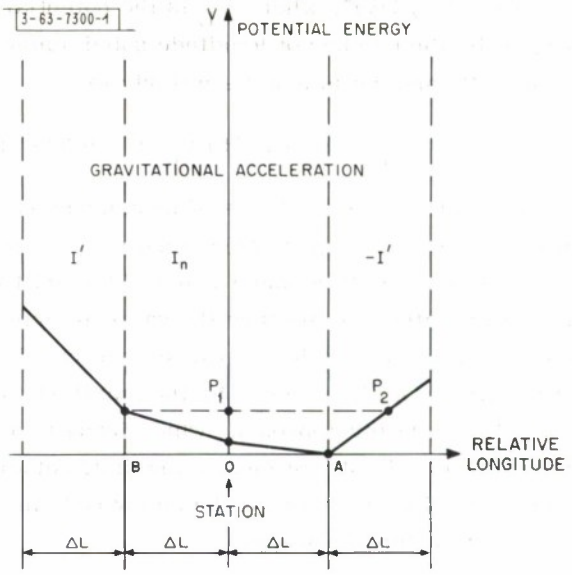

Fig. 11. Potential energy for the second system.

where $\xi_3 \equiv (\alpha_n + |\sin 2\delta|)^{\frac{1}{2}}$, and the limit for $\sin 2\delta \to 0$ is

$$Q_o^{(2)} = 2\alpha_n F_c/(1.5 + \alpha_n/\alpha') \quad . \tag{V-28}$$

c. Comparison of the Two Systems

Comparing Eqs. (V-26) and (V-28) yields $Q_o^{(2)} < Q_o^{(1)}$ for $\alpha_n < \frac{1}{2}\ \alpha'$. It has been seen that α' must exceed unity to ensure the existence of a potential minimum in a neighborhood of the station. Also, α_n must be less than unity to make the residual energy V_R small. In general, this inequality is satisfied and the second system is preferable when $f_c = 0$. For instance, for $\alpha' = 2$ and $\alpha_n = \frac{1}{4}$, $Q_o^{(1)} = 0.4\ F_e$ and $Q_o^{(2)} = 0.308\ F_e$. The second system is superior when the external force is zero or sufficiently small. As $\alpha_n \to 0$, $Q_o^{(2)}/Q_o^{(1)} \to \frac{2}{3}$. When the external force is maximum, i.e., $|\sin 2\delta| = 1$, then $Q^{(1)} = 1.27\ F_e$ and $Q^{(2)} = 1.16\ F_e$. Therefore, the second system consumes less fuel also when the force is maximum. Notice that when $\alpha_n \to 0$, $Q^{(1)}$ and $Q^{(2)}$ tend to f_e, i. e., the systems tend to a minimum fuel system in which the impulse per orbit applied by the motor equals the acceleration per orbit due to the external force. It is therefore possible to conclude that:

(1) The second system is superior.

(2) The impulse $I' = \alpha' F_e$ should be the smallest compatible with the requirement of being sufficiently greater than F_e to give some safety margin. A good value is approximately $\alpha' = 2$, the final selection being made on the basis of convenience in the electronic implementation.

(3) The impulse I_n in the last step of the damping cycle should be as small as possible.

3. Active Damping

After the satellite has acquired a station, its kinetic energy is decreased by an active damping system. A first requirement is to have a high potential wall (Fig. 7) which makes it impossible for the satellite to return to the station acquisition mode. This determines the width L of the tracking band and the impulse level between $+\Delta L$ and $-L$, since it must be, from (V-5),

$V_L \geq 0.088\ (\text{deg/day})^2$, where V_L is the potential energy at a longitude $\pm L$ from the station. Letting h be the number of longitude subdivisions of width ΔL in which the applied impulse has the value I'', and defining α'' similarly to α',

$$V_L = (\alpha' + \alpha'' h)\, F_e \Delta L \geq 0.088\ (\text{deg/day})^2 \quad . \tag{V-29}$$

Since ΔL is chosen on the basis of measurement errors and of system requirements, and α' was obtained previously, Eq. (V-29) determines the product $\alpha'' h$.

To obtain a small residual value of the drift velocity at the end of the damping process, it is necessary either to measure the satellite drift velocity accurately or to reduce the damping impulse adaptively. In the first case, the residual drift velocity is determined by the measurement accuracy; in the second, by the smallest value of damping force which can be used in practice.† The latter approach, which leads to a sequential design of the controller, was taken because of the difficulty of measuring drift velocities.

Two damping systems will be compared, in which successive values of the damping impulse obey a relationship of the type

$$I_k = \pm I_o a^{-k} \quad , \quad a > 1 \quad , \tag{V-30}$$

and the sign is chosen so as to oppose the drift velocity. The two systems differ in the manner in which the transition from I_k to I_{k+1} occurs:

(a) Zero Crossing Adaptation: The transition from I_k to I_{k+1} occurs at each zero crossing, i.e., each time the measured position of the satellite passes from region A to A' in Fig. 8, or vice versa.

(b) Convergence Adaptation: The transition from I_k to I_{k+1} occurs each time the satellite converges to the band $\pm \Delta L$ around the station. In general, several zero crossings can occur before convergence.

In studying both systems, the initial kinetic energy will be taken to equal V_L from (V-29) for $\alpha' = 2$, $a'' = 6$, and $h = 6$. The following analysis is therefore a worst-case study of convergence time. Two definitions are useful in the study of the active damping system. The convergence time is the time after which the total energy (in the λ variable) V_L remains below a small value V_R which is the residual energy toward which the system is designed to converge. The damping efficiency is the ratio of the initial kinetic energy (in the λ variable) of the satellite to the energy (in the λ variable) expended by the thruster in getting the total energy below V_R.

Zero Crossing Adaptation:— In this system, the damping impulse is divided by a factor $a > 1$ every time the satellite passes through zero. After k half oscillations of the system, the total energy is

$$V_k = V_L - \alpha_o F_e \Delta L \sum_{i=0}^{k-1} a^{-i} \quad , \quad k \geq 1 \quad , \tag{V-31}$$

where $\alpha_o F_e$ is the initial damping impulse. The sequence is ended when

$$V_n < \alpha_o a^{-n} F_c \Delta L \quad , \tag{V-32}$$

† Energy is coupled into the system by errors in determining the boundaries of longitude bands, as discussed in the following.

or

$$V_L - \alpha_o F_e \Delta L \sum_{i=0}^{n-1} a^{-i} < \alpha_o a^{-n} F_e \Delta L \quad . \tag{V-33}$$

Using (V-29) and executing the summation in (V-33), rearranging and letting $a^{-n} = \epsilon$, the condition for convergence is

$$\alpha_o > 38(a - 1)/(a - \epsilon) \quad . \tag{V-34}$$

When this condition is not satisfied, the rate of decrease of the damping impulse is too great in relation to that at which energy is subtracted from the system, and convergence does not occur. If α_o can be increased sufficiently, inequality (V-34) can always be satisfied. However, the initial damping force α_o cannot be arbitrarily large. The operation of the adaptive damping system will eventually be limited by the accuracy of the longitude measurement, since a longitude error δL in establishing the boundary of the damping band causes a variation of the potential energy of the system

$$\delta V = \alpha_o F_e \delta L \quad . \tag{V-35}$$

Requiring that δV be smaller than some percentage η of V_L, an upper bound for α_o is determined; e.g., for $\delta L = 0.25°$ and $\eta = 2\%$, $\alpha_o \leqslant 6$. Using this condition in (V-34), $a \leqslant 1.19 - 6\epsilon/32$. Obviously, operating with these low values of a is not very efficient. The energy expended by the active damper on the satellite is

$$W = 2V_L + 2V_1 + \ldots + 2V_n = 2V_L + 2 \sum_{k=1}^{n} V_k \tag{V-36}$$

or, from (V-31),

$$W = 2(n + 1) V_L - 2\alpha_o \frac{a(n + 1)}{a - 1} F_e \Delta L + 2\alpha_o \left(\frac{a}{a - 1}\right)^2 (1 - a^{-(n+1)}) F_c \Delta L \quad . \tag{V-37}$$

For example, if $\epsilon = 1/32$, which is a reasonable value to have a sufficiently small I_n, $n \cong 19$. With the values $n = 19$, $\alpha_o = 6$, $V_L = 38 F_e \Delta L$, and $a = 1.18$, the damping efficiency, from (V-37), is $\eta_D = 0.085$.

Convergence Adaptation:— In this type of damping controller, α_k is retained until the satellite is trapped in the damping band $\pm \Delta L$ wide around the origin. In the rest of this section, the most efficient damping sequence is determined for dampers of the second type. Consider a damping sequence in which $V_n = V_o a^{-n}$, $a > 1$. The first convergence is obtained after N_o half-cycles of satellite position. From the previous definitions and for $V_L = 38 F_e \Delta L$, the energy expended during this first phase is

$$\begin{aligned} W' &= 2V_L + 2(V_L - V_o) + 2(V_L - 2V_o) + \ldots + 2[V_L - (N_o - 1) V_o] \\ &= 2N_o V_L - N_o(N_o - 1) V_o \quad . \end{aligned} \tag{V-38}$$

After the first convergence, the number N of half-cycles of satellite position necessary to obtain each successive partial convergence obviously is the smallest integer $\geqslant (a - 1)$. The energy W'' expended is then, for $a \geqslant 2$,

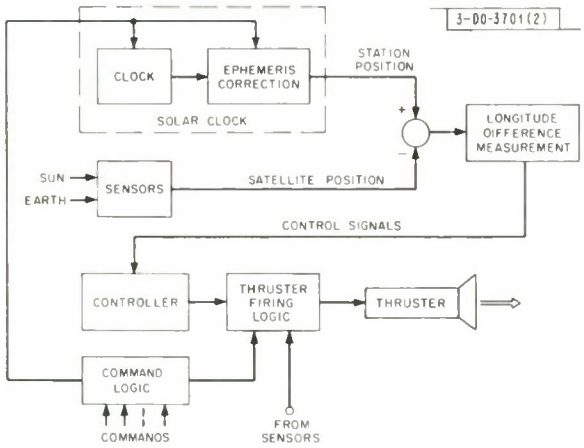

Fig. 12. Simplified block diagram of the Automatic Orbit Control system for LES-6.

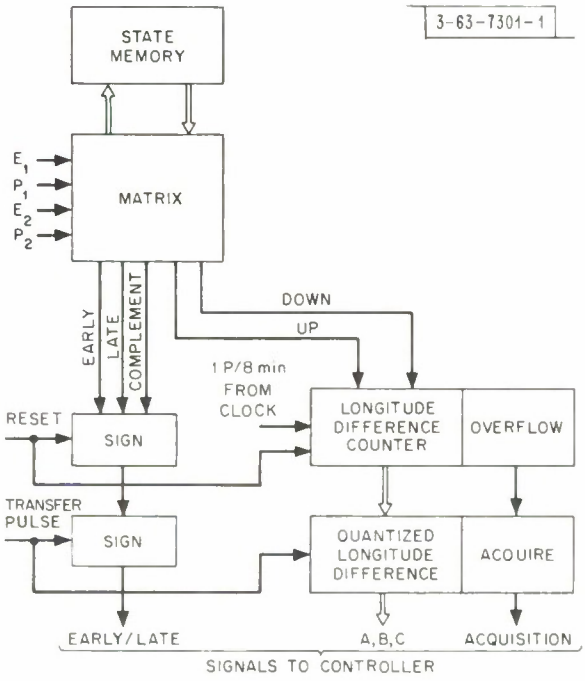

Fig. 13. Block diagram of longitude measurement logic.

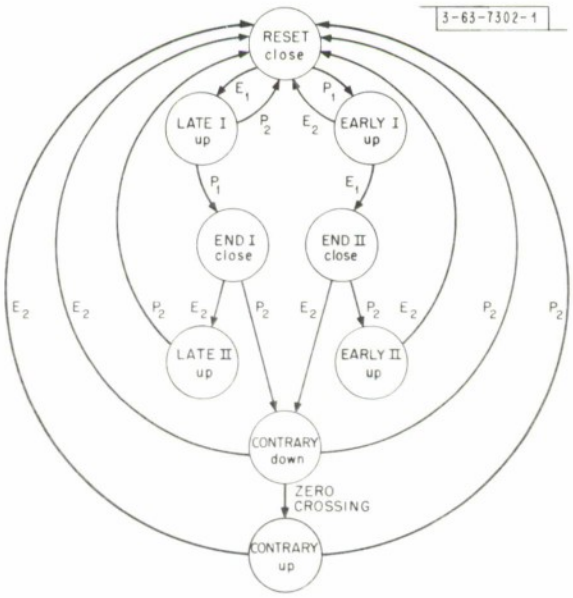

Fig. 14. Flow diagram of longitude measurement logic.

$$W'' = 2N \sum_{i=0}^{n-1} V_i = 2Na(a-1)^{-1}(1-\epsilon)V_o \quad . \tag{V-39}$$

The lowest value of W'' is obtained for a = 2. Since the energy W' is independent of a, the optimum is obtained when a = 2. Using (V-38), (V-39), and recalling that $V_L = 38 F_e \Delta L$, $V_o = \alpha_o F_e \Delta L$, and $N_o = 38/\alpha_o$,

$$\eta_D = 38 \Big/ \left[\frac{38^2}{\alpha_o} + 38 + 2(1-\epsilon)\alpha_o \frac{Na}{a-1} \right] \quad , \tag{V-40}$$

which yields $\eta_D = 0.13$ for $\alpha_o = 6$, a = 2, $\epsilon = 1/32$, and N = 1. Notice from (V-39) that, if l_o could be made larger, so that $V_o = V_L$, the damping efficiency in the optimum configuration would be

$$\eta_{D\,max} = \frac{a-1}{2(1-\epsilon)Na} \cong 0.25 \quad . \tag{V-41}$$

This efficiency is also obtained whenever the initial energy is small, so that the system always converges in one cycle. The values of the successive damping impulses are then $I_k = -2^{-k} I_o$. Since α_o is selected on the basis of the maximum potential variation caused by measurement errors, the only parameter to be determined is the value ϵ, i.e., the final value l_n, which should be retained after convergence to ensure minimum steady-state fuel consumption and should be as small as is compatible with practical requirements.

VI. REALIZATION, SIMULATION, AND TESTING OF FLIGHT SYSTEM

A. Logic Design of Controller

The over-all block diagram of the stationkeeping system is shown in Fig. 12. The solar clock determines the position of the station which is selected by command from ground. Sun and earth sensors and the associated coincidence circuitry determine the satellite position. The longitude difference in sign and absolute value is stored in a memory. Measurements are made twice per orbit at satellite anomalies 180° apart and averaged. The controller remembers the sequence of longitude difference measurements and determines the required thrust level in accordance with the laws established in Sec. V. The thruster firing logic turns the thruster on so that the resulting thrust vector is always tangential to the orbit and has an appropriate direction. A command from ground can turn the thruster on at any time for the initial orbit adjustments (Sec. III-E). Commands can also be sent to the clock to initiate it to the appropriate day of the year (see Appendix A). The system weight is about 4 pounds and the power consumption is 120 mW.

1. Longitude Difference Measurement

The block diagram of the longitude difference measurement logic is shown in Fig. 13. The inputs are the station and the satellite position signals E_1 and E_2 and P_1 and P_2, respectively. The purpose of the state memory is to discriminate against wrong sequences such as P_1, E_2, P_2, E_1. These sequences can occur at the beginning of the stationkeeping experiment and whenever a station is changed. The system will wait until P_1 or E_1 followed by E_1 or P_1 is received before enabling the longitude counter.

The state memory also determines the sign of the longitude difference measurement by adding algebraically the differences measurements P_1 and P_2, as results from the flow diagram of Fig. 14.

In the Early and Late states the counter counts up. In the Contrary 1 state the counter counts down until it crosses zero, then reverses direction and complements the sign register. The counter has an overflow register which determines when the satellite is out of the tracking band.

The longitude difference measurement is transferred in fixed increments to a secondary memory upon receipt of a transfer pulse which is generated after the second measurement and the thrusting have been completed. The secondary memory contains the information "the satellite is (or is not) in band A, B, C, or in the acquisition band." Signal redundancy techniques are used to avoid a single spurious pulse bringing the controller into the Acquisition Mode.

2. Control Unit

The block diagram of the control unit is shown in Fig. 15. Upon arrival of an Aequisition signal, a pulse train is fed to the firing timer, which opens after the thrust logic has sent an Open signal. The input P_2 is used to count days, since this thrust must be applied for two consecutive days. The opposite thrust is applied when the satellite arrives at the damping band. For redundaney and to avoid false signals, the logic waits for two B signals, or a transition from Early to Late, or viee versa. When either situation oceurs, the opposite thrust is applied for two days; when the thrusting operation is eompleted, the satellite returns to the station tracking mode.

In the tracking mode, the operation of the controller is determined by the sequenees of the inputs A, B, C, together with their "sign" E, L. The "memory-state diagram" for the controller in the tracking mode is shown in Fig. 16. The thrust output is determined by the memory state and by the current value of the quantized longitude; thus several "output states" are eondensed in one "memory state" for simplicity of presentation; the complete output state diagram consists of 61 states. From the aequisition mode the controller goes to the state (Damp $-$) if it is early and to (Damp +) if it is late. In these states no damping force is applied whenever the satellite is in bands +A and $-$A, respeetively. Whenever there is a partial eonvergenee, the

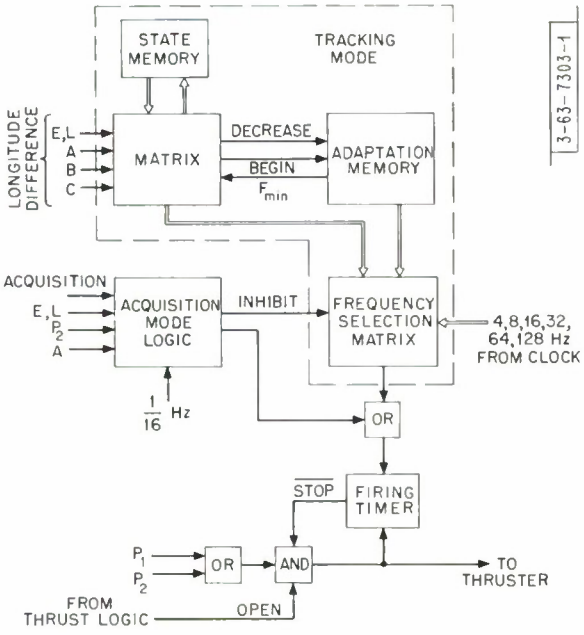

Fig. 15. Block diogrom of the controller.

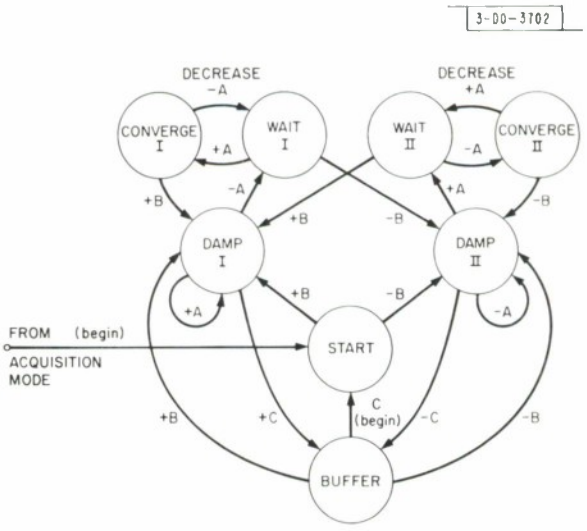

Fig. 16. Memory-stote diogram of the controller.

sequenee – A, +A, – A oecurs if the eontroller is in (Damp –) and the sequenee +A, – A, +A if it is in (Damp +). On the transition from the states Converge to the states Wait, the damping foree is deereased unless it has already reaehed its minimum value. The eontroller exits from the states Converge upon reeeipt of a B signal, and the damping force returns to its maximum value upon reeeipt of the signal Begin, whieh happens after two sueeessive C signals.

The adaptation memory input is the Deerease signal (Fig. 15). The damping foree is obtained by ehoosing a frequeney in the frequency seleetion matrix, whieh is sent to the fixed length firing timer. When the satellite is in bands ±B or ±C, the foree level is established in a similar manner. An Inhibit signal prevents the operation of the traeking-eontrol mode when the satellite is in Aequisition.

When both the firing sequenee and the longitude differenee measurement have been eompleted, a Reset and a Transfer pulse are generated and fed to the auxiliary longitude differenee memory in Fig. 13.

3. Thrust Logic

The thrust logie block diagram is shown in Fig. 17. The earth eenter detector delivers a pulse whenever a fixed marker point on the satellite periphery is eollinear with the earth and satellite eenters. Sinee the firing angle of the thruster is 18°, the thruster line of action is plaeed 81° away from the marker point. After the arrival of the earth eenter pulse, if the satellite is early the thruster is turned on and remains on until the firing angle eounter overflows. The sun clock used to measure the firing angle delivers 512 pulses per satellite spin. If the satellite is late, the thrust must oppose the satellite velocity veetor. A delay of 180° of satellite rotation is therefore introduced before the thruster is turned on.

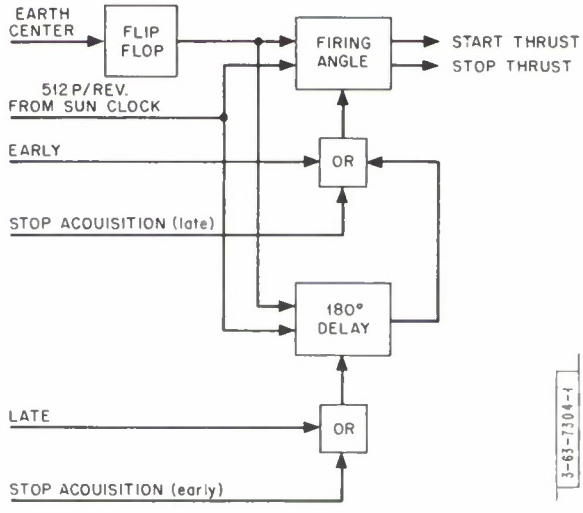

Fig. 17. Thrust logic black diagram.

The logie for the Plasma Thrusters differs from this, in that there are four thrusters located 90° away from eaeh other.[33] The sun eloek is used to gate the appropriate thruster, and the 180° delay selects the direction of firing.

4. Eleetronie Solar Clock

In order to compare the satellite and station positions in orbit, it is necessary to have a solar eloek, as diseussed in Sec. III.

The differenee between the mean and true solar transit times is shown for the year 1969 by the smooth eurve in Fig. 18. It may be assumed that this eurve is valid for subsequent years, sinee the seeular variation of the differenee is small during the satellite lifetime. The clock is a sequential network whieh delays the output of a eounter by a time D (Fig. 18) as shown in the bloek diagram of Fig. 19. Two pulses per mean day, 12 hours apart, start a delay eounter whieh counts minutes until its eontents equal the contents of the accumulator. At this time, the output pulses S_1 or S_2 are generated and the delay eounter is reset and opened until the next pulse from

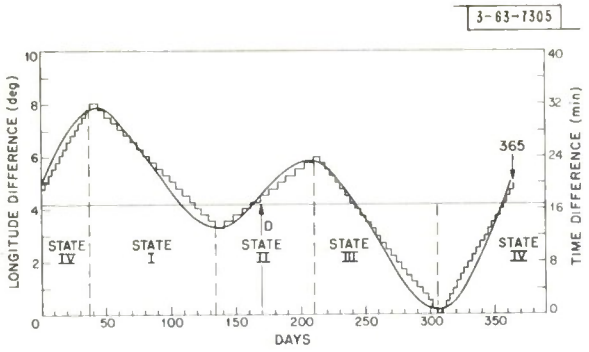

Fig. 18. Approximation to the sun transit time.

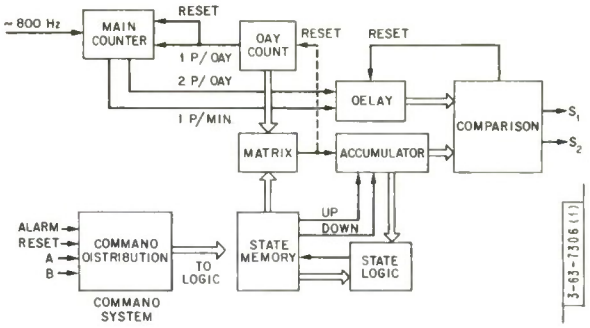

Fig. 19. Block diagram of the electronic solar clock.

the main counter arrives. The accumulator contains the amount of delay measured from the reference line in Fig. 18. As shown, the reference line differs from the mean solar day line by 17 minutes. This is taken into account by sending the alarm command at an appropriate time. The value stored in the accumulator, which is an up-down counter, is computed by the sequential network shown in Fig. 19. The staircase curve in Fig. 18 shows the actual correction obtained with this logic. The approximation has been selected by a trial-and-error procedure, with a view to simplifying the logic design. Since the information contained in the solar clock logic must be preserved when the satellite is in shadow, and the main counter must continue to operate throughout the shadow period, the system is powered from the solar bus or a battery.

The most important function performed by command from ground is the selection of the station. This is done by resetting the main counter at 9 a.m. local mean solar time of the station to be tracked, since the satellite position is measured at 9 a.m. satellite truc solar time. Since the daily correction is obtained as a delay from a reference line 17 minutes earlier than the mean solar day, the time at which the main counter must be reset is 8:43 a.m. station mean solar time. The longitude of the station, the longitude of the command site, and the propagation delays are known and therefore determine the site mean solar time at which the command, which is called ALARM, must be sent. An error in the time at which the ALARM is sent only causes an offset error in the operation of the control system. The magnitude of this offset is obviously 1° of longitude per 4 minutes of time error, so that very reasonable accuracies can be achieved. The command system of the solar clock also performs the auxiliary function of choosing the initial conditions for the sequential network and for the accumulator. This is necessary because the actual date of launch is not exactly known beforehand and is also uscful as an additional element of flexibility in the system.

B. Computer Simulation and Flight System Testing

An extensive computer simulation study was carried out during the program,[34] to yield estimates (1) of the fuel consumption when operating with the cold gas thrusters in the presence of random measurement errors, and (2) of the dynamic behavior. In the course of this work, it was found that it was advantageous to increasc the width of thc B longitude band from 2° to 4°, since this resulted in lower fuel consumption in the presence of random errors. This modification was therefore incorporated in the hardware design.

The Stationkeeping Simulation program performs the following operations for each orbit:

(1) Integration of the equation of motion with earth tesseral harmonics through third order,

(2) Generation of the coincidence pulses at the appropriate sun ephemeris time,

(3) Determination of the satellite position, using the reconstruction of the sun ephemeris implemented by the on-board logic, or by the special sensor,

(4) Adding random error (uniformly distributed, uncorrelated, ±0.5°) to the measurement,

(5) Determination of the thrust level required for the next orbit, using a subroutine which duplicates the behavior of the finite-state controller.

The outputs are the osculating orbital elements for each orbit and the fuel consumption. It is possible to simulate operation with both the Plasma and Cold Gas Thrusters. This simulation program can take as inputs the orbital elements determined by radar tracking.

A variable step-size Hamming's integration routine was used. It is important to use a variable step-size method because of the discontinuous nature of the forces involved. Much work was done to study the effect of integration errors.† This is most important, since the number of successive integrations is quite large when the simulation is carried on for the equivalent of five years of orbital life. In order to handle discontinuous thrust properly, one would like to use a small step size; this, however, increases the number of necessary integration steps. An appropriate compromise was found and its validity checked by comparing the results given by Hamming's and Runge-Kutta variable step-size routines.

An extensive analysis of fuel consumption was made for different values of the stationkeeping longitude. Uniformly distributed uncorrelated noise was used, since it seemed a sufficiently severe test for the system.

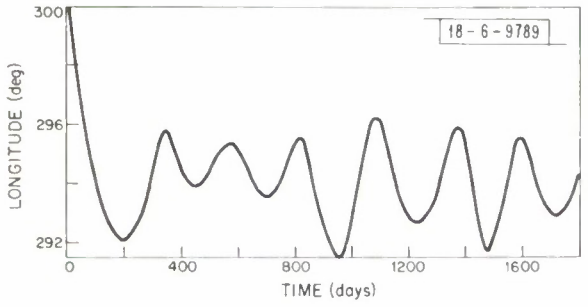

Fig. 20. Simulation results at the worst longitude.

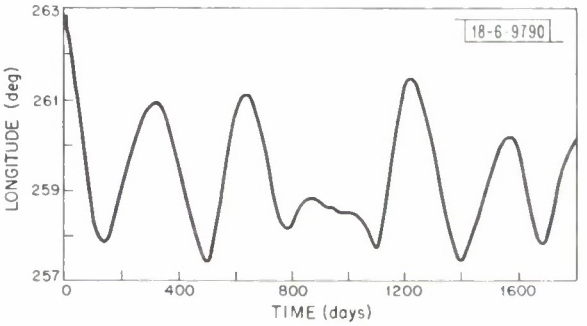

Fig. 21. Simulation results at the unstable point.

The design constraint of not being able to measure the angular drift except in very largely quantized longitude bands mades the system rather sensitive to fast, uncorrelated noise. The reason for this is that the controller can go very rapidly through the damping cycle, as a consequence of spurious sequences of signals like +A, −A, +A or −A, +A, −A. As is seen in Sec. V, the controller responds to this sequence by switching to a lower level damping force. Figures 20 and 21 show typical computer runs for stationkeeping at the worst longitude (~295° East) and at the unstable point (~259° East) with the Cold Gas Thrusters, with random error. In most cases, the longitudinal excursion is within ±3 degrees of the station.

Several runs were made to estimate the fuel consumption in the presence of random errors. As is to be expected, the fuel consumption is a function of the stationkeeping longitude. Typically,

† E. H. Swenson, unpublished report.

the system will use 2.6 kg when stationkeeping for five years near a point of maximum tangential force, and 0.6 kg near the unstable point.

Testing of the system was carried out by exciting the earth and sun sensors using a special-purpose Simulator. This device simulated sequences of sun and earth pulses at the spin rate of the satellite. Circular orbital motion was simulated by changing the sun-earth phase uniformly in time. The Simulator had provisions to change the orbital speed and to "jump" to any point in orbit using pushbuttons. The stationkeeping system clock could be sped up, so that the Day Pulses would occur with variable repetition rates, down to as little as 1 minute. In this manner, by measuring the time elapsing between the Day Pulses E_1, E_2, which were available externally via telemetry, the "satellite position" on the simulator could be changed so that the sensor coincidences P_1, P_2 would occur at the appropriate times with respect to the clock. By changing the time between E_1 and P_1 (E_2, P_2) for a given clock speed, the system measures different longitudes. This type of checkout was conducted also during thermal-vacuum tests.

A second technique, which was most useful in testing the integration of the sensors and logic systems, was employed in which the satellite was actually spinning. The light from a lamp sun simulator (appropriately folded by mirrors) was used to excite the sun sensors. The earth image was projected on screens in such a manner as to obtain approximately the right earth albedo. The earth image could be moved (discontinuously) so that sensor coincidences could be obtained at the right time with respect to the clock pulses also in this case.

VII. EARLY FLIGHT RESULTS AND COINCIDENCE ANALYSIS

The longitude history of the satellite from 26 September 1968 until 25 June 1969 is shown in Fig. 22. The Automatic Stationkeeping System operated from 22 December 1968 to the end of the period. Telemetry was recorded daily from the Automatic System longitude sensors. The ephemeris transit time has been subtracted from the sensor data.

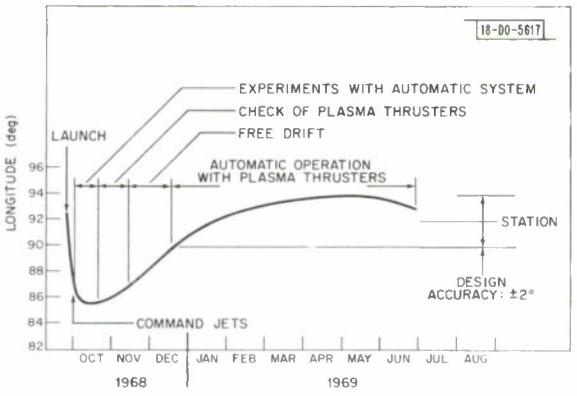

Fig. 22. Longitude history of LES-6 since launch, as measured by the on-board equipment daily (smoothed data).

Orbit determinations were made (independently of the sensor data) once a month, and more frequently for calibration purposes at the beginning of the experiment. These are indicated by the open circles in Fig. 22.

During the period from launch to 22 December 1968, the system operated mostly in the "Ground Command" mode. During this time the following operations were performed: (a) initial trimming of the orbit, using the Cold Gas Thrusters, (b) experimentation with the Plasma Thrusters, to determine their thrust level, and (c) experimentation with the Automatic System, closing the loop for brief periods of time and monitoring its behavior continuously.

All operations were performed suceessfully. The initial orbit (semimajor axis 42,068 km; eeeentrieity 0.00226; drift rate +1.21°/day) was trimmed to a nearly synehronous orbit (semimajor axis 42,159 km; eeeentrieity < 0.0001; drift rate 0.051°/day). The thrust obtained from the Gas Thrusters was found to be within 10 pereent of the ground measurements.

The Plasma Thrusters have established a reeord of operation in orbit for eleetrie propulsion systems. The measurement of their performanee required long periods of operation, and thus elimination of the natural perturbations from the motion. This is beeause the effeet of the Plasma Thrusters is quite eomparable in magnitude to that of the geopotential perturbation. The thrust value obtained was very elose to the value measured on the ground.[33]

The quiet period from 12 November to 22 Deeember was neeessary to eheek our orbit determination teehniques by predieting motion under the effeet of the natural perturbations only. Our 30-foot antenna and reeeiver installation ean measure satellite range (via time delay measurements through the satellite repeater) very aeeurately, besides measuring azimuth and elevation. We now believe that our orbit determination aeeuraey is of the order of 0.3 km in semimajor axis (typical 3σ value).

The Automatie System was turned on for a long-term experiment on 23 Deeember 1968. At this time the satellite had a drift rate of 0.062 deg/day west. At this longitude the geopotential perturbation tends to move the satellite west. The Alarm Command was sent to locate the station at about 80° West, so that a C-band measurement would be made by the on-board system. This resulted in slowing down the satellite, as seen from Fig. 22 and recorded by the orbit determinations of 17 January and 20 February (drift rate of 0.026 deg/day). If the Automatie System had not operated, the drift rate at this time would have been about 0.5 deg/day. On 18 February the station was moved to 92.5° West longitude.

The data obtained from the sensors were analyzed to test several hypotheses about their distribution. Figure 23 shows the actual unsmoothed data for the period 8 January to 5 March 1969.

To test the validity of the "weak-eoupling" approximation to the drift motion, we made least-square fits of polynomials of time to the data. The results, summarized in Table II, show that the unbiased estimate of the variance of the residuals is either increased or not significantly decreased in going from a second degree to a third degree fit. Thus the weak eoupling approximation, whieh predicts a near parabolic behavior for small longitude excursions [see Eq. (II-35)], is supported. The seeond degree least square fit is seen in Fig. 23 (continuous curve).

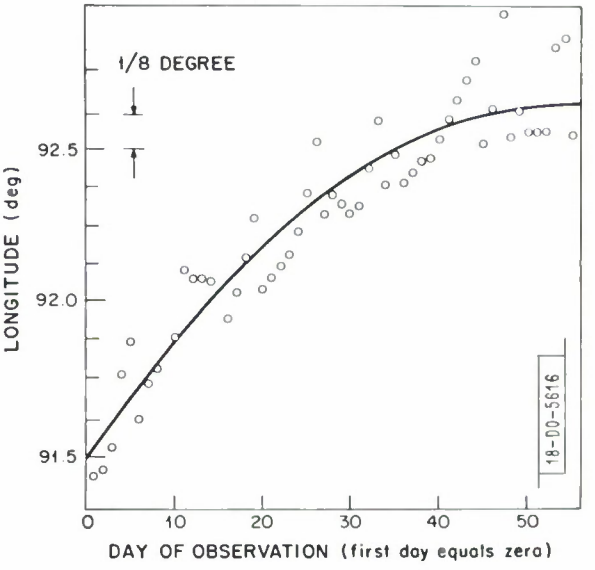

Fig. 23. Position meosured by the on-board equipment in a typicol period of operotion.

Next we studied the residuals, having eliminated the trend via the parabolie least-square fit.

Stationarity:— The variance of the residuals is different in the different periods, as shown in Table II. Furthermore, one can see periods in which the data scatter is greater, even though the daily thrust has not changed compared to a relatively quiet period (typically, the

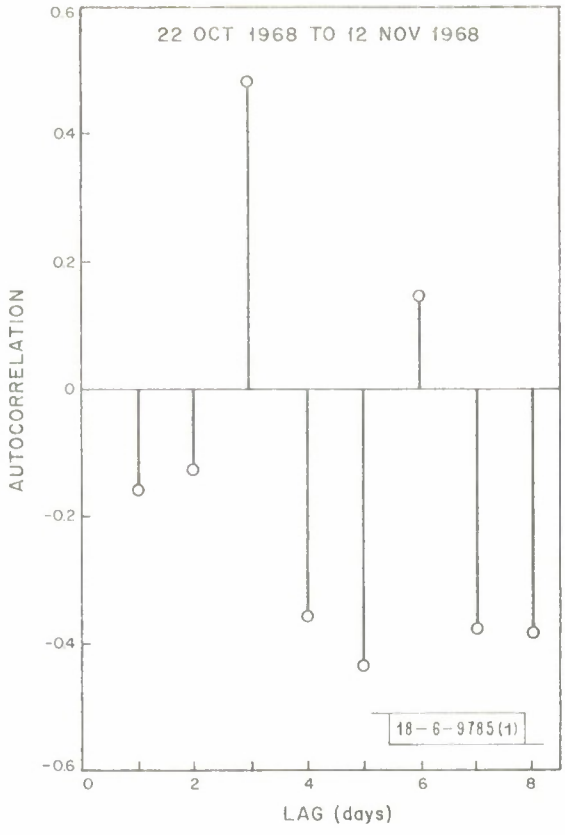

Fig. 24. Autocorrelotion of the sensor errors (first period).

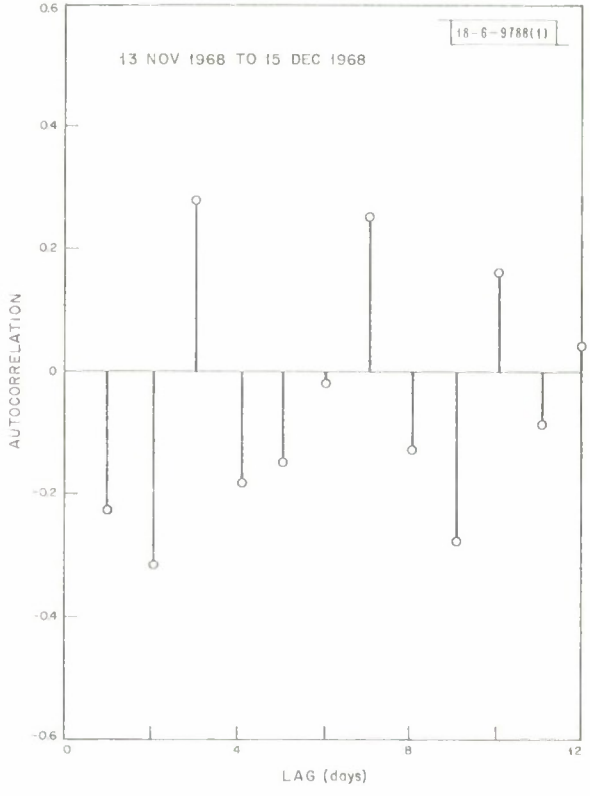

Fig. 25. Autocorrelotion of the sensor errors (second period).

TABLE II VARIANCE OF RESIDUALS				
Period	Linear Fit (sec)	Parabolic Fit (sec)	3rd Degree Polynomial (sec)	4th Degree Polynomial (sec)
First (22 Oct.-12 Nov.)	15.15	11.42	10.93	11.59
Second (12 Nov.-15 Dec.)	32.32	28.87	29.16	31.67
Third (23 Dec.-7 Jon.)	61.98	62.03	63.05	64.40
Fourth (8 Jan.-13 Feb.)	39.63	33.04	32.26	32.16

third and fourth periods). The difference in variance strongly supports the hypothesis that the residuals are not weakly stationary (and thus not stationary) in time.

Whiteness:- We applied Anderson's modified test for whiteness, which is applicable if the residuals are uncorrelated. This is done by computing the autocorrelation for unity lag for the sample from the time series. The results for the autocorrelation function are shown in Figs. 24 through 27. We also applied the Durban Watson test for whiteness to the different periods. To gain some intuitive "feel" for the behavior of the autocorrelation function for truncated time series obtained from a "white" process, we repeated the analysis for samples obtained from

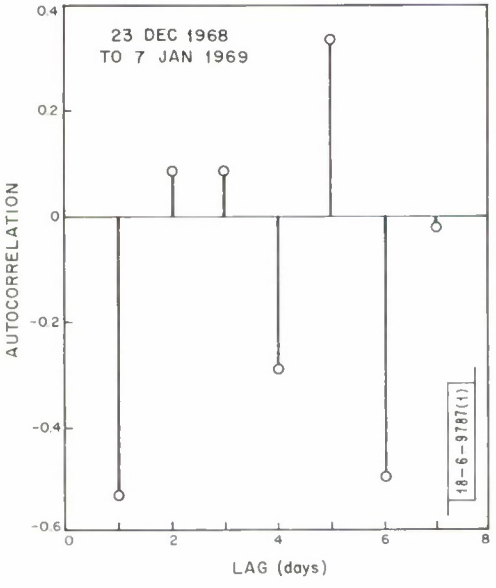

Fig. 26. Autocorrelotion of the sensor errors (third period).

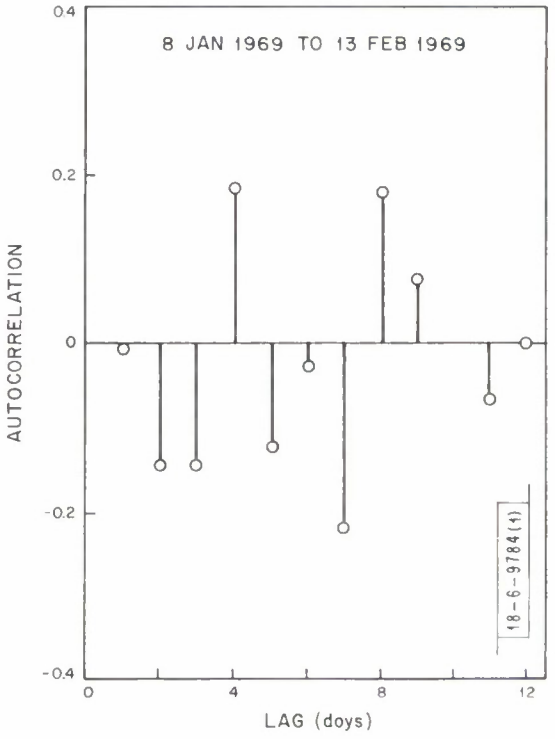

Fig. 27. Autocorrelation of the sensor errors (fourth period).

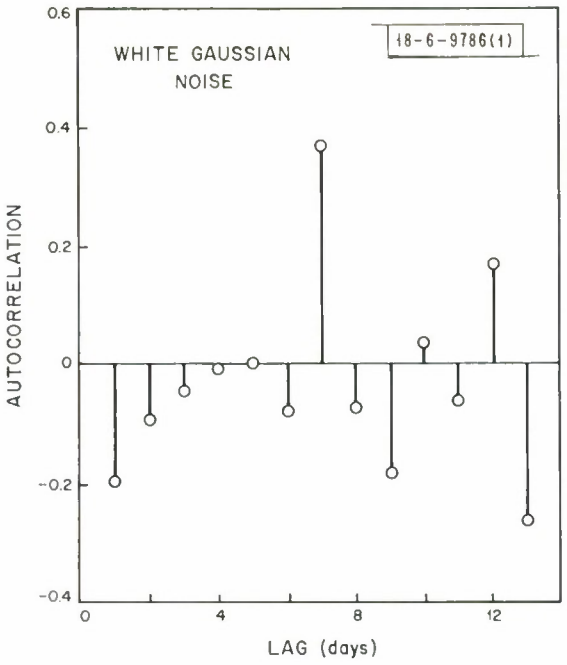

Fig. 28. Autocorrelation function for white Goussian noise.

white Gaussian noise and uncorrelated equiprobable noise. A typical result is shown in Fig. 28. We conclude that our analysis of the data available so far supports the hypothesis that the residuals are a white random process.

Hystograms:– To obtain some information on the underlying probability function, we prepared hystograms of the residuals. The hystograms are often bimodal; only in periods III and IV do the hystograms show a behavior reminiscent of the Gaussian curve. In order to interpret the meaning of the residuals, it is important to note that the telemetry sampling rate is about 20 seconds. Thus there is an intrinsic uncertainty of about 0.1 degree in the measurement. The information on the distribution will be improved as the available measurement sample increases in time.

VIII. CONCLUSIONS

The Automatic Orbit Control system of LES-6 had operated successfully for several months at the time of this writing. The main conclusions to be drawn from this experience are, in our opinion:

(1) It is possible to automatically control synchronous orbits with modest equipment complexity. This leads to simplification of ground operations and reduction in operating costs of networks of synchronous satellites.

(2) The accuracy of control, which in the present experiments appears to be of a few degrees, should improve in future systems.

(3) From a control-theoretic point of view, it is important to notice the advantages of symmetric measurements and thrusting, which ensure the stability of the coordinates which are not controllable when the satellite longitude is sampled once per day.

The data presented here describe the first few months of operation of the LES-6 automatic system, using the Plasma Thrusters. Experiments of station transfer and of prolonged operation with the Gas Thrusters will be carried out in the near future.

In the author's opinion, methods of Automatie Orbit Control will be used extensively on tomorrow's synehronous satellites. This judgment is based on the faet that the number of satellites in synchronous orbit will almost eertainly inerease greatly. Stationkeeping requirements will then be dietated by the need to avoid interference between synchronous satellites. The need for Automatie Orbit Control is not limited to the synehronous orbit. Both eireular nonsynchronous and general elliptie earth orbits are perturbed by the geopotential harmonies, the sun and the moon. The system that has been flown in LES-6 is only a beginning; more aeeurate on-board eontrol of synehronous orbits should be possible on the next generation of satellites. We also see these ideas extended and applied to more eomplex problems of orbit eontrol.

ACKNOWLEDGMENTS

The realization and integration of this system required the eooperation of many people in the Spaee Teehniques Group of Lineoln Laboratory under the leadership of Dr. H. Sherman. In partieular, D. C. MaeLellan, D. M. Nathanson, and W. J. Guman† were responsible for the propulsion systems (an ammonia thruster system and four pulsed plasma thrusters[33]). Professor R. W. Broekett of M. I. T. eonsulted with us on many problems throughout the study. M. C. Croeker‡ and E. H. Swenson did most of the simulation work, and F. S. Zimnoeh earried out the data reduetion. J. H. Helfrieh eondueted part of the final testing and system doeumentation. The author was responsible for the system design and for the development and testing of the digital eontroller, with the assistance of R. F. Williams. The author is especially grateful to Professor Brockett for permission to use the results of Ref. 27 in Sees. IV-A and IV-B.

† Fairchild Hiller Corporatian, Farmingdale, New Yark.

‡ Presently at Amerieon Sciene and Engineering, Cambridge, Massaehusetts.

REFERENCES

1. L. Blitzer, et al., "Effect of Ellipticity of the Equator on 24-Hour Nearly Circular Satellite Orbits," J. Geophys. Res. 67, 329 (1962).
2. P. Musen and A. E. Bailie, "On The Motion of a 24-Hour Satellite," J. Geophys. Res. 67, 1123 (1962).
3. R. R. Allan, "Perturbations of a Geostationary Satellite by the Longitude-Dependent Terms in the Earth's Gravitational Field," Planet. Space Sci. 11, 1325 (1963).
4. C. A. Wagner, "The Drift of a 24-Hour Satellite due to an Earth Gravity Field through Fourth Order," NASA Technical Note D-2103 (February 1964).
5. _____, "The Drift of an Inclined-Orbit 24-Hour Satellite in an Earth Gravity Field through Fourth Order," NASA Technical Note D-3316 (May 1966).
6. J. S. Gansler, "Space Navigation," TNB General Precision Aerospace 8, 1st Quarter, 1965.
7. _____, "Mechanization of a Self-Contained Navigation System," PTG SET Record Paper No. 5.3, IEEE 1963 National Space Electronics Symposium.
8. R. H. Gersten and Z. E. Schwarzbein, "Self-Contained Orbit Determination Techniques," in Celestial Mechanics and Astrodynamics, V. G. Szebehely, Ed. (Academic Press, New York, 1964), pp. 683-708.
9. _____, "Preliminary Orbit Determination from Self-Contained Data," AIAA J. 2, 751 (1964).
10. D. F. McAllister and J. T. Wagner, "Lunar and Earth Orbital Navigation," J. Brit. Interplanet. Soc. 19, 521 (November-December 1964).
11. K. N. Satyendra and R. E. Bradford, "Self-Contained Navigational System for Determination of Orbital Elements of a Satellite," J. Am. Rocket Soc. 31, 949 (1961).
12. J. D. McLean, S. F. Schmidt and L. A. McGee, "Optimal Filtering and Linear Prediction Applied to a Space Navigation System for the Circum-Lunar Mission," NASA Technical Note D-1208 (March 1962).
13. R. H. Battin, "A Satatistical Optimizing Navigation Procedure for Space Flight," J. Am. Rocket Soc. 32, 1681 (1962).
14. M. Frazier, B. Kriegsman and F. W. Nesline, Jr., "Self-Contained Satellite Naviation Systems," AIAA J. 1, 2310 (1963).
15. A. L. Knoll and M. M. Edelstein, "Estimation of Local Vertical and Orbital Parameters for an Earth Satellite Using Horizon Sensor Measurements," AIAA J. 3, 338 (1965).
16. T. L. Gunckel and J. C. Elsey, "Fixed Point Simulation of On-Board Orbit Determination," J. Spacecraft Rockets 4, 885 (1967).
17. J. H. Hutcheson and F. T. Smith, "An Orbital Control Process for a 24-Hour Communication Satellite," The RAND Corporation, Research Memorandum RM-2809-NASA (October 1961).
18. F. T. Smith and J. A. Burkhart, "An Optimal Orbital Control Process for a 24-Hour Communication Satellite," The RAND Corporation, Research Memorandum RM-3255-NASA (July 1962).
19. F. T. Smith, "A Set of Two-Body Orbital Parameters Useful for Nearly Circular Orbits and Some Related Equations," The RAND Corporation, Research Memorandum RM-3037-NASA (February 1962).
20. _____, "A Differential Correction Process for Near-Circular Orbits," The RAND Corporation, Research Memorandum RM-3037-NASA (February 1962).
21. A. A. Braga-Illa, "Orbit Determination from the Satellite," J. Spacecraft Rockets 6, 232 (1969).
22. M. Jeffreys, The Earth, 4th ed. (Cambridge University Press, 1959).
23. P. Kendall and R. Stalcup, "Attitude Reference Devices for Space Vehicles," Proc. I. R. E. 48, 765 (1960).
24. B. Kovit, "I. R. Horizon Sensor Guides Planetary Orbiting," Space and Aeronautics 35, 131 (1961).
25. H. Sherman, D. C. MacLellan, R. M. Lerner and P. Waldron, "Lincoln Experimental Satellite Program (LES-1, -2, -3, -4)," J. Spacecraft Rockets 4, 1448 (1967).

26. D. Brouwer and G. M. Clemence, Methods of Celestial Mechanics (Academic Press, New York, 1961), Ch. 2.

27. R. Brockett, "The Controllability and Observability of Satellites in Near-circular Orbits," unpublished report (May 1967).

28. P. Hempel and J. Tschauner, "Besuhlepnigungsprogramme Mimimaler Ubergangsenergie fur des Rendezvous-Manover," Astronautica Acta 10, 221 (1964).

29. J. S. Meditch, J. L. LeMay and J. P. Janus, "Analysis of an Horizon Scanner Autonomous Orbital Navigation System," TDR-469 (5540-10)-6, Aerospace Corporation (July 1965).

30. I. B. Chammas, "Least-Squares Design of Orbit Controller," M. S. Thesis, Massachusetts Institute of Technology, Cambridge, Massachusetts (May 1968).

31. B. J. Moriarty, "Position Error in Station-Keeping Satellite," Technical Note 1966-21, Lincoln Laboratory, M.I.T. (1 April 1966), DDC AD-633034.

32. A. A. Braga-Illa, "Automatic Satellite Stationkeeping," J. Spacecraft Rockets 6, 4 (1969).

33. W. J. Guman and D. M. Nathanson, "Pulsed Plasma Microthruster Propulsion System for Synchronous Orbit Satellite," AIAA Paper No. 69-298, 7th Electric Propulsion Conference, Williamsburg, Virginia (March 1969).

34. M. Crocker, "A Simulation of Automatic Stationkeeping for Synchronous Satellites," AAS/AIAA Astrodynamics Specialist Conference, 3-5 September 1968.

APPENDIX A
THE SOLAR TIME ON AN ARBITRARILY ORIENTED SATELLITE

If it is assumed that the earth's and satellite's spin axes are parallel, the transit of the sun on corresponding meridian planes of the two bodies occurs at times inversely proportional to their spin rates. This is no longer so if the spin axes are not parallel. The variation of meridian transit time has two major causes: the inclination of the plane of the elliptic to the equatorial body of the earth or satellite, and the ellipticity of the earth's orbit, with which the satellite's orbit around the sun can be assumed to coincide in our approximation.

In the following, formulas are given for the difference between mean solar time and true solar time measured on a satellite arbitrarily oriented in an orbit of any inclination, eccentricity, and period. The satellite orbital inclination does not affect the satellite solar time unless errors are made in sensing the earth. The formulas take the earth's orbit eccentricity into account to second order, and are easily extended to higher order.

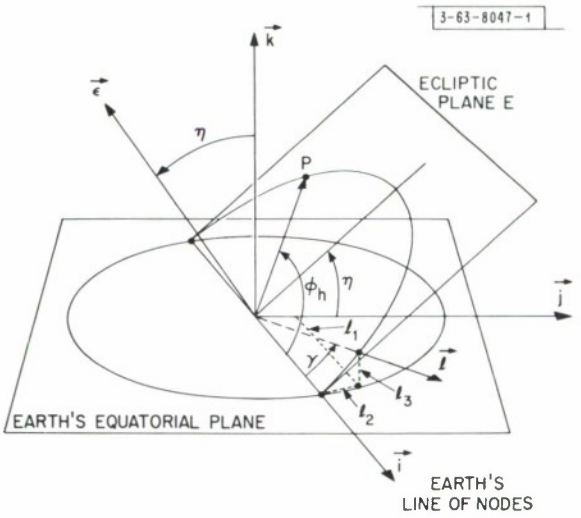

Fig. A-1. Satellite reference system.

The reference system used is shown in Fig. A-1. The unit vectors i, j are in the earth's equatorial plane, and i coincides with the direction of the earth's node. The triad i, j, k is right-handed. The ecliptic plane E is defined by the direction cosines, e$\{u_1, u_2, u_3\}$; α is the angle between the ecliptic plane E and the satellite equatorial plane, U, not shown in the figure; β is the angle between plane U and the orbital plane; ϵ and ϵ_E are the eccentricities of the satellite and earth orbits, respectively; $\omega = 2\pi$ rad/sidereal year; Ω = satellite orbital radian frequency; $\varphi_h = 102.25°$ = argument of perihelion measured from the earth's nodal line.

The coincidence in time between the output of the earth and sun sensor will occur when the projections of the satellite and of the sun differ by δ, which is the angular separation between the earth and sun sensor, and an integer number of rotations.

Then the times of successive coincidences are found to be the solutions of the equation

$$\tan^{-1}[\cos(\alpha)\tan(\omega t + \varphi_h)] + \frac{2\epsilon_E \sin(\omega t)\cos(\alpha)}{1 - \sin^2(\alpha)\sin^2(\omega t)} = \tan^{-1}[\cos(\beta)\tan(\Omega t + \varphi_{so})]$$

$$+ \frac{2\epsilon \sin(\Omega t)\cos(\beta)}{1 - \sin^2(\beta)\sin^2(\Omega t)} + \delta + 2n\pi \quad . \tag{A-1}$$

No loss in generality occurs if one takes $\delta = 0$, which displaces the time reference.

Let us now take as a reference for Eq. (A-1) that at which the first coincidence for $t = 0$, $n = 0$ occurs at perihelion for a satellite spin or yaw axis normal to the earth's equatorial plane. Then $u_1 = u_2 = 0$ and $u_3 = 1$ in (A-2) and from (A-1),

$$\varphi_{so} = \tan^{-1}\left[\frac{\cos(\alpha)}{\cos(\beta)}\tan\varphi_h\right] \quad . \tag{A-2}$$

The expression (A-2) is substituted into (A-1). The times of coincidence are the solutions of Eq. (A-1) in the unknown t, for different integer values of n.

It is of interest to consider some special cases and to rewrite Eq. (A-1) in ways more convenient for the applications.

For a synchronous satellite, the quantities ω and Ω can be expressed in rad/mean solar day as $\omega = 2\pi\xi$, $\Omega = 2\pi(1 + \xi)$, and $\xi \cong 1/365.27$. Measuring the time in mean solar days, it is more convenient to consider the angular difference Δ between the satellite and sun projection on plane U at the end of each successive mean solar day. Then,

$$\Delta = \varphi_s - \tan^{-1}\left[\cos(\alpha)\tan(2\pi\xi n + \varphi_h)\right] - \frac{2\epsilon_E \sin(\omega t)\cos(\alpha)}{1 - \sin^2(\alpha)\sin^2(\omega t)} \quad , \tag{A-3}$$

where φ_s is given by the right side of (A-1) with $\Omega = 2\pi(1 + \xi)$ and with φ_{so} given by (A-2).

For a synchronous equatorial satellite in a circular orbit with its spin or yaw axis perpendicular to the equatorial plane of the earth, Eq. (A-3) yields an approximate expression for the sun transit time correction on the earth Δ_E, being

$$\beta = 0 \quad , \qquad \xi \cong 1/365.27 \quad ,$$

$$\epsilon = 0 \quad , \qquad \varphi_h \cong 102.25° \quad ,$$

$$u_1 = u_2 = 0 \quad , \qquad \epsilon_E \cong 0.01675 \quad ,$$

$$\alpha = \eta \cong 23.45° \quad , \qquad u_3 = 1 \quad .$$

$$\Delta_E = 2\pi\xi n + \varphi_{so} - \tan^{-1}\left[\cos(\eta)\tan(2\pi\xi n + \varphi_h)\right] - \frac{2\epsilon_E \sin(2\pi\xi n)\cos(\eta)}{1 - \sin^2(\eta)\sin^2(2\pi\xi n)} \quad . \tag{A-4}$$

For a synchronous equatorial satellite in a circular orbit with its spin or yaw axis tilted around the earth's line of nodes, the foregoing values are used, except that, ψ being the angle of tilt,

$$u_1 = 0 \quad ,$$

$$u_2 = -\sin(\psi) \quad ,$$

$$\cos(\alpha) = \sin(\eta)\sin(\psi) + \cos(\eta)\cos(\psi) = \cos(\eta - \psi) \quad ,$$

and

$$\Delta\psi = 2\pi\xi n + \varphi_{so} - \tan^{-1}\left[\cos(\eta - \psi)\tan(2\pi\xi n + \varphi_h)\right] - \frac{2\epsilon_E \sin(2\pi\xi n)\cos(\eta - \psi)}{1 - \sin^2(\eta - \psi)\sin^2(2\pi\xi n)} \quad . \tag{A-5}$$

Comparing this equation with (A-4), one sees that a rotation of the yaw axis around the earth's line of nodes is equivalent to a rotation of the plane of the ecliptic around the same line. This means that the satellite solstices and equinoxes take place on the same day as the earth's, as is obvious from the fact that the lines of nodes of satellite and earth still coincide. Plots of angular displacement vs time of the year for this case are shown in Fig. A-2.

For a synchronous equatorial satellite in a circular orbit with its yaw axis tilted around the normal to the earth's line of nodes, and with χ being the angle of tilt,

$$u_1 = -\sin(\chi) \quad , \quad u_2 = 0 \quad , \quad u_3 = \cos(\chi) \quad , \quad \cos(\alpha) = \cos(\chi)\cos(\eta) \quad ,$$

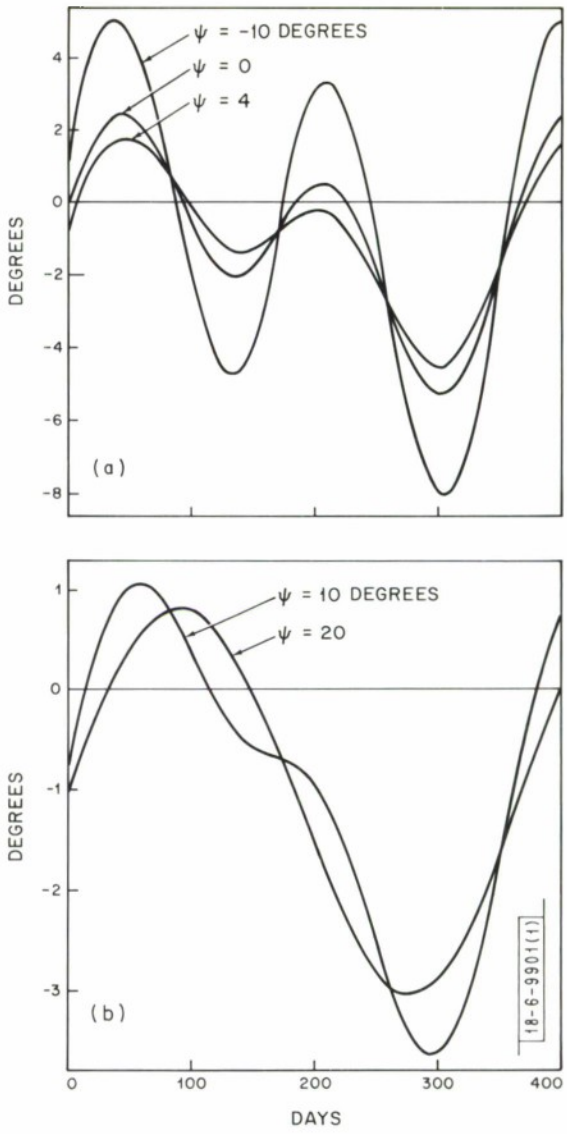

Fig. A-2. Solar time as seen an the sotellite for different angles of tilt.

and therefore

$$\Delta_\chi = + 2\pi\xi n + \varphi_{so} - \tan^{-1}\left[\cos(\eta)\cos(\chi)\tan(2\pi\xi n + \varphi_h)\right]$$

$$- \frac{2\epsilon_E \sin(2\pi\xi n)\cos(\chi)\cos(\eta)}{\cos^2(2\pi\xi n) + \cos^2(\eta)\cos^2(\chi)\sin^2(2\pi\xi n)} \quad . \tag{A-6}$$

From (A-1) and $\Omega = 2\pi(1 + \xi)$, the eccentricity of the satellite orbit is seen to contribute the term

$$\Delta' = \frac{2\epsilon \sin[2\pi(1 + \xi) n]\cos(\beta)}{1 - \sin^2(\beta)\sin^2[2\pi(1 + \xi) n]} \quad . \tag{A-7}$$

This confirms that the eccentricity effect can be eliminated to second order in ϵ by taking two measurements of satellite solar time at times n and n + (1/2), being

$$\Delta'(n) \simeq - \Delta'[n + (\tfrac{1}{2})] \quad ,$$

since ξ is small.

APPENDIX B
THE OBSERVABILITY AND CONTROLLABILITY MATRICES FOR THE SAMPLED CASE†

The sampled case equations are given by

$$\underline{x}(kT + T) = \underline{A}_s\underline{x}(kT) + \underline{B}_s\underline{u}(kT) \quad , \tag{B-1}$$

and the measured vector is

$$\underline{y}(k) = \underline{C}\underline{x}(k) \quad , \tag{B-2}$$

where the matrices $\underline{A}_s$ and $\underline{B}_s$ are given by Eqs. (IV-20), (IV-21), (IV-22) for the different cases.

The system is again factored into two parts and we can examine both separately.

i. Case $T = 2\pi/\omega$ (sampling once per orbit)

If $u_2 = 0$,

$$\underline{K}_1 = \begin{bmatrix} 0 & 0 & 0 & 0 \\ 1 & 1 & 1 & 1 \\ 0 & 0 & 0 & 0 \\ 0 & 0 & 0 & 0 \end{bmatrix} \tag{B-3}$$

This is singular so that the sampled system is not controllable from u_1. (Actually, we could have inferred this from the continuous case.)

Let us check the case $T = 2\pi/\omega$ and $u_1 = 0$. Here we have

$$\underline{K}_2 = \begin{bmatrix} 0 & 0 & 0 & 0 \\ 0 & 0 & 0 & 0 \\ \frac{-6\pi}{\omega} & \frac{-12\pi}{\omega} & \frac{-18\pi}{\omega} & \frac{-24\pi}{\omega} \\ 1 & 1 & 1 & 1 \end{bmatrix} \tag{B-4}$$

and we see that sampling at the rate $T = 2\pi/\omega$ has destroyed controllability from u_2.

If we wish to check controllability from both u_1 and u_2 together, the relevant matrix is

† From Ref. 27.

$$\underline{K}_3 = \begin{bmatrix} 0 & 0 & 0 & 0 & 0 & 0 & 0 & 0 \\ 1 & 0 & 1 & 0 & 1 & 0 & 1 & 0 \\ 0 & \frac{-6\pi}{\omega} & 0 & -12\pi & 0 & \frac{-18\pi}{\omega} & 0 & \frac{-24\pi}{\omega} \\ 0 & 1 & 0 & 1 & 0 & 1 & 0 & 1 \end{bmatrix} \tag{B-5}$$

which is also singular. Hence, even with both u_1 and u_2 available one cannot control if only one thrust per orbit is used.

The controllability of x_5 and x_6 from u_3 is revealed by

$$\underline{K}_4 = \begin{bmatrix} 0 & 0 \\ 1 & 1 \end{bmatrix} \tag{B-6}$$

which is singular and hence indicates a lack of controllability.

The observability picture is as follows. From x_1 we have an observability matrix

$$\underline{L}_1 = \begin{bmatrix} 1 & 0 & 0 & 0 \\ 1 & 0 & 0 & 0 \\ 1 & 0 & 0 & 0 \\ 1 & 0 & 0 & 0 \end{bmatrix} \tag{B-7}$$

From x_3 we have an observability matrix of the form

$$\underline{L}_2 = \begin{bmatrix} 0 & 0 & 1 & 0 \\ -12\pi & 0 & 1 & \frac{-6\pi}{\omega} \\ -24\pi & 0 & 1 & \frac{-12\pi}{\omega} \\ -36\pi & 0 & 1 & \frac{-18\pi}{\omega} \end{bmatrix} \tag{B-8}$$

and from x_1 and x_3 together we have

$$\underline{L}_3 = \begin{bmatrix} 1 & 0 & 0 & 0 \\ 0 & 0 & 1 & 0 \\ 1 & 0 & 0 & 0 \\ -12\pi & 0 & 1 & \frac{-6\pi}{\omega} \\ 1 & 0 & 0 & 0 \\ -24\pi & 0 & 1 & \frac{-12\pi}{\omega} \\ 1 & 0 & 0 & 0 \\ -36\pi & 0 & 1 & \frac{-18\pi}{\omega} \end{bmatrix} \tag{B-9}$$

Clearly none of these matrices is of rank 4 so we cannot observe the inplane components of the motion using one observation per orbit.

The out-of-plane situation is revealed by

$$\underline{L}_4 = \begin{bmatrix} 1 & 0 \\ 1 & 0 \end{bmatrix} \tag{B-10}$$

so we see that this motion is not observable either.

ii. Case $T = \pi/\omega$ (sampling twice per orbit)

In this case, the controllability matrices $\underline{K}_1$, $\underline{K}_2$, and $\underline{K}_3$ take the form

$$\underline{K}_1 = \begin{bmatrix} 0 & 0 & 0 & 0 \\ -1 & 1 & -1 & -1 \\ \frac{-4}{\omega} & 0 & \frac{-4}{\omega} & 0 \\ 0 & 0 & 0 & 0 \end{bmatrix} \tag{B-11}$$

$$\underline{K}_2 = \begin{bmatrix} \frac{4}{\omega} & 0 & \frac{4}{\omega} & 0 \\ 0 & 0 & 0 & 0 \\ \frac{-3\pi}{\omega} & \frac{-6\pi}{\omega} & \frac{-9\pi}{\omega} & \frac{-9\pi}{\omega} \\ -7 & 1 & -7 & 1 \end{bmatrix} \tag{B-12}$$

$$\underline{K}_3 = \begin{bmatrix} 0 & \frac{4}{\omega} & 0 & 0 & 0 & \frac{4}{\omega} & 0 & 0 \\ -1 & 0 & 1 & 0 & 1 & 0 & -1 & 0 \\ \frac{-4}{\omega} & \frac{-3\pi}{\omega} & 0 & \frac{-6\pi}{\omega} & \frac{-4}{\omega} & \frac{-9\pi}{\omega} & 0 & \frac{-9\pi}{\omega} \\ 0 & -7 & 0 & 1 & 0 & -7 & 0 & 1 \end{bmatrix} \tag{B-13}$$

Both $\underline{K}_1$ and $\underline{K}_2$ are singular, but $\underline{K}_3$ is of rank 4 (the first four columns are independent). Hence, it is possible to control the in-plane motion by thrusting only twice per orbit, provided that one has both tangential and radial thrusting capability.

For the out-of-plane motion, the situation is not improved, however, because

$$\underline{K}_4 = \begin{bmatrix} 0 & 0 \\ -1 & 1 \end{bmatrix} \tag{B-14}$$

and is not of rank 2.

As far as observability is concerned, we have

$$\underline{L}_1 = \begin{bmatrix} 1 & 0 & 0 & 0 \\ 7 & 0 & 0 & \frac{4}{\omega} \\ 1 & 0 & 0 & 0 \\ 7 & 0 & 0 & \frac{4}{\omega} \end{bmatrix} \tag{B-15}$$

$$\underline{L}_2 = \begin{bmatrix} 0 & 0 & 1 & 0 \\ -6\pi & \frac{-4}{\omega} & 1 & \frac{-3\pi}{\omega} \\ -12\pi & 0 & 1 & \frac{-6\pi}{\omega} \\ -18\pi & 0 & 1 & \frac{-9\pi}{\omega} \end{bmatrix} \tag{B-16}$$

$$\underline{L}_3 = \begin{bmatrix} 1 & 0 & 0 & 0 \\ 0 & 0 & 1 & 0 \\ 7 & 0 & 0 & \frac{4}{\omega} \\ -6\pi & \frac{-4}{\omega} & 1 & \frac{-3\pi}{\omega} \\ 1 & 0 & 0 & 0 \\ -12\pi & -8\omega & 1 & \frac{-6\pi}{\omega} \\ 7 & 0 & 0 & \frac{4}{\omega} \\ -18\pi & -12\pi\omega & 1 & \frac{-9\pi}{\omega} \end{bmatrix} \tag{B-17}$$

Only matrix L_3 is of rank 4 (the first four rows are independent). Hence the in-plane motion is observable, sampling only twice per orbit if both angle and altitude can be measured.

For the out-of-plane motion, we need to examine

$$\underline{L}_4 = \begin{bmatrix} 1 & 0 \\ 1 & 0 \end{bmatrix} \tag{B-18}$$

and we see that this part of the system is still not observable.

iii. Case $T = \pi/2\omega$ (sampling four times per orbit)

The controllability matrices $\underline{K}_1$, $\underline{K}_2$, and $\underline{K}_3$ are now given by

$$\underline{K}_1 = \begin{bmatrix} \frac{1}{\omega} & 0 & \frac{-1}{\omega} & 0 \\ 0 & -1 & 0 & 1 \\ \frac{-2}{\omega} & \frac{-4}{\omega} & \frac{-2}{\omega} & 0 \\ -2 & 0 & 2 & 0 \end{bmatrix} \tag{B-19}$$

$$\underline{K}_2 = \begin{bmatrix} \frac{2}{\omega} & \frac{4}{\omega} & \frac{2}{\omega} & 0 \\ 2 & 0 & -2 & 0 \\ \frac{(-3\pi+8)}{2\omega} & \frac{-3\pi}{\omega} & \frac{(-9\pi-8)}{2\omega} & \frac{-6\pi}{\omega} \\ -3 & -7 & -3 & 1 \end{bmatrix} \tag{B-20}$$

$$\underline{K}_3 = \begin{bmatrix} \frac{1}{\omega} & \frac{2}{\omega} & 0 & \frac{4}{\omega} & \frac{-1}{\omega} & \frac{2}{\omega} & 0 & 0 \\ 0 & 2 & -1 & 0 & 0 & -2 & 1 & 0 \\ \frac{-2}{\omega} & \frac{(-3\pi+8)}{2\omega} & \frac{-4}{\omega} & \frac{-3\pi}{\omega} & \frac{-2}{\omega} & \frac{(-9\pi-8)}{2\omega} & 0 & \frac{-6\pi}{\omega} \\ -2 & -3 & 0 & -7 & 2 & -3 & 0 & 1 \end{bmatrix} \tag{B-21}$$

In this case, $\underline{K}_2$ and $\underline{K}_3$ are of rank 4 but $\underline{K}_1$ is not. Thus, controlling the Θ dependent variable only lets one control the entire state if thrusting is done four times per orbit.

For the out-of-plane motion, $\underline{K}_4$ takes the form

$$\underline{K}_4 = \begin{bmatrix} \frac{1}{\omega} & 0 \\ 0 & -1 \end{bmatrix} \tag{B-22}$$

Thus this motion is controllable.

To check observability in the four times per orbit sampled case, we need

$$\underline{L}_1 = \begin{bmatrix} 1 & 0 & 0 & 0 \\ 4 & \frac{1}{\omega} & 0 & \frac{2}{\omega} \\ 7 & 0 & 0 & \frac{4}{\omega} \\ 4 & \frac{-1}{\omega} & 0 & \frac{2}{\omega} \end{bmatrix} \tag{B-23}$$

$$\underline{L}_2 = \begin{bmatrix} 0 & 0 & 1 & 0 \\ (-3\pi + 6) & \frac{-2}{\omega} & 1 & \frac{(-3\pi + 8)}{2\omega} \\ -6\pi & \frac{-4}{\omega} & 1 & \frac{-3\pi}{\omega} \\ -9\pi - 6 & \frac{-2}{\omega} & 1 & \frac{(-9\pi - 8)}{2\omega} \end{bmatrix} \tag{B-24}$$

$$\underline{L}_3 = \begin{bmatrix} 1 & 0 & 0 & 0 \\ 0 & 0 & 1 & 0 \\ 4 & \frac{1}{\omega} & 0 & \frac{2}{\omega} \\ (-3\pi + 6) & \frac{-2}{\omega} & 1 & \frac{(-3\pi + 8)}{2\omega} \\ 7 & 0 & 0 & \frac{4}{\omega} \\ -6\pi & \frac{-4}{\omega} & 1 & \frac{-3\pi}{\omega} \\ 4 & \frac{-1}{\omega} & 0 & \frac{2}{\omega} \\ -9\pi - 6 & \frac{-6}{\omega} & 1 & \frac{(-9\pi - 8)}{2\omega} \end{bmatrix} \tag{B-25}$$

Clearly, $\underline{L}_1$ is not of rank 4 so we cannot observe the state by looking at altitude alone. However, $\underline{L}_2$ and $\underline{L}_3$ are of rank 4, so observation from Θ, and from r and Θ together, is possible.

The out-of-plane motion is covered by

$$\underline{L}_4 = \begin{bmatrix} 1 & 0 \\ 0 & \frac{1}{\omega} \end{bmatrix} \tag{B-26}$$

and it is observable from four samples of φ per orbit.

DOCUMENT CONTROL DATA - R&D

(Security classification of title, body of abstract and indexing annotation must be entered when the overall report is classified)

1. ORIGINATING ACTIVITY *(Corporate author)* Lincoln Laboratory, M.I.T.	2a. REPORT SECURITY CLASSIFICATION Unclassified 2b. GROUP None

3. REPORT TITLE

Automatic Orbit Control of the Lincoln Experimental Satellite LES-6

4. DESCRIPTIVE NOTES *(Type of report and inclusive dates)*

Technical Report

5. AUTHOR(S) *(Last name, first name, initial)*

Braga-Illa, Alvise A.

6. REPORT DATE	7a. TOTAL NO. OF PAGES	7b. NO. OF REFS
10 July 1969	64	34

8a. CONTRACT OR GRANT NO. AF 19(628)-5167 b. PROJECT NO. 649 L c. d.	9a. ORIGINATOR'S REPORT NUMBER(S) Technical Report 469 9b. OTHER REPORT NO(S) *(Any other numbers that may be assigned this report)* ESD-TR-69-203

10. AVAILABILITY/LIMITATION NOTICES

This document has been approved for public release and sale; its distribution is unlimited.

11. SUPPLEMENTARY NOTES	12. SPONSORING MILITARY ACTIVITY
None	Air Force Systems Command, USAF

13. ABSTRACT

This report discusses the autonomous orbit control system launched aboard the synchronous communications satellite LES-6 in late 1968. The topics presented include the motivation for automatic orbit control, the measurement techniques, observability and controllability, the design of a variable limit-cycle system, automatic station acquisition, simulation, and testing. The history of the development of this control system is emphasized, and the early flight results are discussed.

14. KEY WORDS

satellite
LES-6
satellite stationkeeping
orbit control
automatic orbit control
digital control systems
controllability
observability